

Computational study and Characteristics of In₂S₃ thin films: Effects of substrate nature and deposition temperature

Kawther Assili^{1,3*}, Wafa Selmi², Khaled Alouani¹, Xavier Vilanova³

¹ University of Tunis El Manar, Faculty of Science, Laboratory of Analytical Chemistry and Electrochemistry, Campus, 2092 Tunis, Tunisia.

* Corresponding author: e-mail: kawther.assili@fst.utm.tn

assoulakawther@gmail.com

² University of Tunis El Manar, Faculty of Science, Laboratory of materials crystal chemistry and applied thermodynamics, Campus, 2092 Tunis, Tunisia.

³ University Rovira i Virgili, Department of Electronic, Electrical and Automatic Engineering, 43007 Tarragona, Spain.

Highlights:

- First report on the chemical vapor growth of β -In₂S₃ thin films using Triphenylphosphine sulfide as a sulfur precursor.
- Effects of growth temperature and substrate nature on the properties of indium sulfide films were investigated.
- β -In₂S₃ films showed good optical properties, useful for optoelectronic and photovoltaic applications.
- DFT calculation show that the composition of the band edge structure of β -In₂S₃ is the key factor of its excellent optical performance.

Abstract

In this work, we investigate the effects of both growth temperature and substrate nature on different properties of indium sulfide thin films prepared by chemical vapor deposition method using triphenylphosphine sulfide as a sulfur precursor. The structural, morphological, and optical properties of the resulting thin films were characterized using X-ray Diffraction (XRD), Scanning Electron Microscopy (SEM) and UV–Vis Spectroscopy respectively. The structural study has proved that pure nanocrystalline β -indium sulfide films were obtained at 300 and 400 °C regardless the substrate nature, while higher growth temperature (500 °C) leads the formation of pure indium oxide films. From the SEM images, it is derived that the surface morphology of the obtained films was independent to both growth temperature and

substrate nature. The electronic structure of β - In_2S_3 was computed using density functional theory calculations. The optical properties of the obtained films such as energy band-gap, extinction coefficient, refractive index, dielectric constant and optical conductivity were investigated theoretically and experimentally. It was shown that these parameters were mainly controlled by the substrate type and the phase formed. The theoretical optical investigation was in fully agreement with the experimental results. Oscillator energy, dispersion energy and Urbach energy were also estimated. Blue and violet PL emission indicate the useful application of the obtained films as blue and violet light emitter.

KEYWORDS: Indium sulfide films; CVD; Ph_3PS , optical properties, DFT calculation.

1. Introduction

Organophosphorus compounds have been classed as one of the main groups in phosphorus chemistry. Through the diversity of their structures and functions, these compounds appears as an interesting support in several areas. This is undoubtedly due to the excellent coordination properties shown for most of the transition metals, the ease and modularity of their synthesis, as well as the stability and interesting dielectric properties they have [1-2].

Thereby, in recent years the literature evidence suggests that organo-chalcogeno-phosphorus compounds could be successful chalcogen precursors in the development of thin film materials. As a matter of fact, the use of these compounds has posed new challenges for several research groups. Therefore, a variety of phosphorus compounds have been exploited to deposit binary semiconductor materials such as: dichalcogeno-imidodiphosphate molecules and its derivatives $\text{R}_2(\text{E})\text{PNHP}(\text{E})\text{R}_2$ ($\text{E} = \text{O}, \text{S}, \text{Se}, \text{Te}$, $\text{R} = \text{alkyl}, \text{aryl}, \text{alkoxy}$) [3], cyclohexylphosphine compounds as $(\text{C}_6\text{H}_{11})\text{PH}_2$ [4], triphenylphosphine chalcogenide as Ph_3PS [5] and Ph_3PSe [6]. Others phosphorus complexes such as $[\text{Pb}((\text{S})\text{PPh}_2)_2\text{N}]_2$, $[\text{Pb}((\text{Se})\text{PPh}_2)_2\text{N}]_2$ [7] $[\text{Sb}(\text{S}_2\text{P}(\text{OR})_2)_3]$ [8], $[\text{In}(\text{iPr}_2\text{PSe}_2)_3]$ and $[\text{Cu}_4(\text{iPr}_2\text{P}_2\text{Se}_2)_4]$ [9] have been also used as single-source precursor. We are therefore witnessing the genesis of a large number of semiconductor materials based on organophosphorus precursors such as: PbS , InP , Sb_2S_3 , In_2Se_3 , Cu_{2-x}Se , SnTe ...

Moreover, the choice of the methodology of deposition is a very critical step, because it should be compatible with the precursor nature and substrate type, to ensure the high quality of the resulting materials [10]. In fact, the choice of the process is based on certain precursor criteria

such as volatility, stability and acid-base character, but also depends on the ease detachment of chalcogen. Therefore, we found that the vapor deposition process is the most adaptable technique that allows the use of the above-mentioned precursors. Particularly, CVD method is a relatively cheap technique and it allows the deposition of a wide range of materials. The main advantage of this technique is the achievement of good coverage and homogenous films onto a large variety of substrates, allowing the possible integration of the obtained films on diverse applications area. Thus, many research groups were particularly interested in this method.

Until today, CVD method was applied to deposit a wide variety of semiconductor materials such as: Co_3O_4 [11], ZrO_2 [12], RuO_2 [13], SnO_2 [14], In_xS_y [15], TiO_2 [16], MoS_2 [17], ZnO [18] ... Among them, indium sulfide in its different forms was classed as a promising candidate for several application fields due to its optical [19], photo-electrochemical [20], electrical [21], acoustical [22] and structural [23] properties. In fact, indium sulfide is a III-VI material formed by non-toxic elements and it can exist in different stoichiometric forms as InS , In_6S_7 , InS_4 , and In_2S_3 . Due to the higher stability, In_2S_3 phase is the most usual. It can be found in three allotropic phases: cubic- α (stable above 420 °C), tetragonal- β (stable below 420 °C) and hexagonal- γ (stable above 750 °C) [24]. Depending on the preparation method and experimental conditions, β - In_2S_3 has a wide band gap energy, ranging from 2 to 3.7 eV, electrical conductivity between 10^{-1} and $10^7 \Omega\cdot\text{cm}$ and always presenting n-type behavior [25]. The carrier concentration and mobility were found to be between 10^{15} – 10^{18} cm^{-3} and 0.2 – $5 \text{ cm}^2 \text{ V}^{-1} \text{ s}^{-1}$ respectively [26].

The effect of film thickness on structural, electrical and optical properties of thermally evaporated In_2S_3 was carried out by Chander et al. [27]. Authors demonstrate that absorption, extinction coefficient and energy band gap decrease with thickness. They conclude that film with 68 nm of thickness can be used as a buffer layer in solar cell applications due to their ideal band gap. Structural and optical studies of In_2S_3 films were investigated as a function of substrate and annealing temperature [28]. The energy band gap of the resulting films decrease with increasing annealing temperature. The electrical properties of indium sulfide films were reported by Revathi et al. [29]. They proved that the obtained films were n-type and their electrical conductivity decrease with substrate temperature. Authors related the decrease in conductivity to the presence of defects into the films.

Keeping in view the different indium sulfide reports, In_2S_3 properties can be influenced by several factors such as growth method, growth temperature, annealing temperature, precursor nature... Reviewing the available literature, one can realize that different compounds have been used as precursor to deposit In_2S_3 thin films including Indium chloride, thioacetamide [30], Indium granules, sulfur powder [31], Indium sulfide powder [32], thiourea [33] and In_2S_3 ceramic target [34]. Using these precursors, In_2S_3 films were grown onto different substrates such as ITO [35], glass [36], silicon [37] and SnO_2 [38]. Nevertheless, no paper can be found using triphenylphosphine sulfide as a sulfur precursor. Moreover, the effect of substrate nature on the properties of this material has not been detailed yet. For this reason, we have investigated the growth of In_2S_3 thin films onto two different substrates (glass and silicon) by CVD using Ph_3PS for the first time. Consequently, the aim of the present study was to probe the effect of substrate nature and growth temperature on the In_2S_3 films properties. The structural, morphological and optical properties of the obtained films were investigated. Hereafter, the electronic band structure of $\beta\text{-In}_2\text{S}_3$, that is rather scarce, will be computed to further fundamental phenomena comprehension.

2. Experimental

2.1. Precursors

Triphenylphosphine sulfide was purchased from Fluka AG and employed without any supplementary purification. Indium targets was 2.00" Diameter x 0.125" thick and with 99.99% purity.

2.2. Sputtering deposition

Before the sulfidization process, a pure indium layer was deposited on both types of substrate. To deposit this Indium layer with a 100 nm thickness, an ATC Orion 8-HV DC magnetron sputtering system with a power of 100 W was used. The deposition was performed at 3 mTorr of vacuum pressure, with a 20 sccm flow of Argon during 550 s.

2.3. Growth of Indium sulfide thin films

The sulfidization of Indium layers was carried out by chemical vapor deposition (CVD) method. The CVD process was operated at different temperatures for 60 min. A 100 sccm flow of Argon

was used as inert carrier gas. More details about the CVD process can be found in our previous papers [5, 39].

2.4. Characterization details

The structural characterization of the obtained films was monitored by a Bruker-AXS D8Discover diffractometer equipped with a $\text{CuK}\alpha$ radiation which the Bragg's angle varying from 20 to 89°. The material identification was performed using PANalytical X'Pert Pro powder X-ray diffractometer. Films morphology was monitored using scanning electron microscopy (SEM) type Quanta 600 from FEI Company. Transmittance and reflectance data of the films were obtained using VARIAN spectrophotometer with a wavelength range from 250 to 2500 nm. Photoluminescence measurements were recorded using a Photoluminescence Spectrometer (PLS) with He–Cd laser source with excitation of 325 nm and power of 20 mW.

2.5. Computational methodology

Single-crystal diffraction data of $\beta\text{-In}_2\text{S}_3$ [40] was used to perform all calculations through the Cambridge Serial Total Energy Package (CASTEP) codes [41]. The exchange and correlation effects are Perdew–Burke–Ernzerhof (PBE) [42] generalized gradient approximation (GGA) [43].

For expanding the Kohn-Sham wave functions, the planewave cut-off energy was set at 400 eV, while the k-point sampling was set to 1x1x1, with tolerance of 0.1 meV/atom in order to perform the irreducible Brillouin Zone. Broyden-Fletcher-Goldfarb-Shanno (BFGS) method [44] was used with the following convergence criteria: energy change of 2.0×10^{-5} eV per atom, maximum force of 0.05 eV per Å, stress less than 0.01 GPa, and atomic displacement tolerance of 2.0×10^{-3} Å.

Computational study was used to determine theoretical optical parameters such as ϵ_i , ϵ_r , α , n , k and σ_{opt} . The theoretical dielectric functions were computed using the following formula [45, 46]:

$$\epsilon(\omega) = \epsilon_r(\omega) + i\epsilon_i(\omega) \quad (1)$$

$$\epsilon_r(\omega) = 1 + \frac{2}{\pi} P \int_0^{\infty} \frac{\omega' \epsilon_i(\omega')}{\omega'^2 - \omega^2} d\omega' \quad (2)$$

$$\epsilon_i(\omega) = \frac{4\pi^2 e^2}{m^2 \omega^2} \sum_{i,j} \int_{BZ} \langle i|M|j \rangle^2 F_i(1 - F_j) \delta(E_F - E_i - \omega) d^3k \quad (3)$$

where P is the principal value of integral, ω is the frequency, e is the electron charge, m is the free electron mass, i is the initial state, j is the final state, M represents the dipole matrix, F_i is the Fermi distribution function for the i state, and E_i is the energy of an electron in the i state. The theoretical optical absorption coefficient $\alpha(\omega)$ was calculated using both the real $\epsilon_r(\omega)$ and imaginary part $\epsilon_i(\omega)$ of the dielectric function, based on the following relation:

$$\alpha(\omega) = \sqrt{2}\omega \left[\sqrt{\epsilon_r(\omega)^2 + \epsilon_i(\omega)^2} - \epsilon_r(\omega) \right]^{1/2} \quad (4)$$

The theoretical refractive index (n) and extinction coefficient (k) were also computed using the theoretical dielectric function, according to the following expressions [47, 48]:

$$n(\omega) = \frac{\left(\epsilon_r(\omega) + (\epsilon_r^2(\omega) + \epsilon_i^2(\omega))^{\frac{1}{2}} \right)^{\frac{1}{2}}}{\sqrt{2}} \quad (5)$$

and

$$k(\omega) = \frac{\left(-\epsilon_r(\omega) + (\epsilon_r^2(\omega) + \epsilon_i^2(\omega))^{\frac{1}{2}} \right)^{\frac{1}{2}}}{\sqrt{2}} \quad (6)$$

Finally, the theoretical optical conductivity was computed using the following equation:

$$\sigma_{opt} = \sigma_r + i\sigma_i = -i \frac{\omega}{4\pi} (\epsilon - 1) \quad (7)$$

Where, σ_r σ_i are the real and imaginary part of the optical conductivity function, ω is the frequency and ϵ is the dielectric constant.

3. Results and discussion

3.1. Structural study

Figure 1 depicts the X-ray diffraction patterns of the obtained films at different sulfidization temperatures onto glass and silicon substrates respectively.

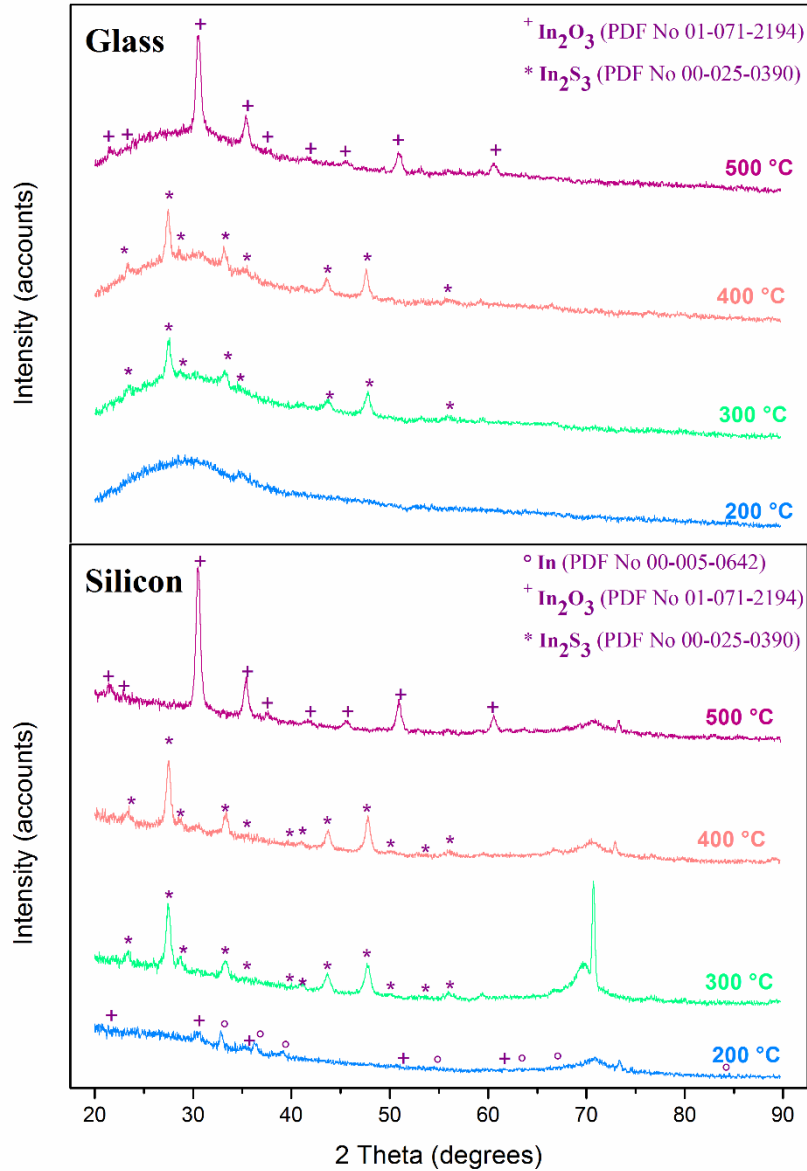


Figure 1. XRD patterns of Indium sulfide thin films prepared at different sulfidization temperature onto glass and silicon substrate.

As shown, according to the growth temperature and the substrate used, we have acquired different diffraction profiles. From Figure 1 it is clear that the film deposited onto glass substrate at 200 °C is amorphous and it has no identified peaks, even those of indium. This may be due to the limited growth, which can be explained by a low thermal energy that may be insufficient to induce the crystallization of the film. Although the deposition conditions were not exactly the same, similar results were obtained by Timouni et al. and by Rasool et al. for indium sulfide thin films deposited by vacuum thermal evaporation method [49, 50]. Nehra et al. obtained also the same amorphous In_2S_3 films onto glass and ITO coated glass

substrates by vacuum evaporation [51]. Authors explain the formation of this amorphous structure by a random arrangement of indium and sulfur atoms into the cell volume.

Increasing the growth temperature to 300 and 400 °C, peaks located at 23°.3, 28°.6, 33°.2, 35°.4, 43°.6, 47°.7, 55°.9 were observed with an intense peak located at 27°.4. The identification of these reflections based on the ICDD database confirms the formation of Tetragonal β - In_2S_3 phase (PDF No 00-025-0390) [52] with a space group I41/amd. The prominent orientation corresponds to (109) plane. The other weak peaks were attributed to (116) (206) (0012) (301) (1015) (2212) (419) planes respectively. Other peaks related to silicon can be observed for films deposited onto silicon substrates at different temperature. The same prominent orientation along (109) was observed for β - In_2S_3 thin films deposited onto glass substrates using $[\text{Et}_2\text{In}(\text{S}_2\text{CNMen}_3\text{Bu})]$ and $\text{In}(\text{SOCNiPr}_2)_3$ precursors by MOCVD technique, regardless the growth temperature used [53]. β - In_2S_3 thin films with (123) preferred orientation were also prepared by Ali Ehsan et al. onto FTO substrate by AACVD method in the range of 300-400°C [54].

It may also be noticed that the peak intensity increases slightly with increasing the sulfidization temperature from 300 to 400 °C, which can indicate that the In_2S_3 formation process pursue yet leading the formation of more compact film. Likewise, Ali Ehsan et al. showed that the peaks intensity increases with increasing the growth temperature, which support our observation. Similar observation was done by Nomura et al. for indium sulfide deposited onto silicon and quartz substrates by MOCVD using $\text{Bu}^n\text{In}(\text{SPri})_2$ [55]. No diffraction peaks were obtained below 300°C, however, β - In_2S_3 phase was identified at 350 and 400°C with a prominent orientation along (103). Contrariwise, Calixto-Rodriguez et al. has shown that no diffraction peak can be identified below 400 °C and β - In_2S_3 was formed only above 400°C [56]. The authors justify the difference between their results and those in the previous reports to the thermodynamic properties of the starting materials. Finally, at 500 °C, all the β - In_2S_3 peaks disappeared and new reflections appear with the more intense one located at 30.6°. The identification of those peaks indicate the formation of pure indium oxide In_2O_3 phase (PDF No 01-071-2194) [57] with Ia-3 space group.

The identification of the diffraction peaks of the films prepared onto silicon substrates at 300 and 400°C show also the formation of the same pure tetragonal β - In_2S_3 phase. In addition, the same oxide phase was identified when film was grown at 500 °C. Nevertheless, at 200 °C, some

new peaks were revealed and attributed to the Tetragonal Indium (PDF No 00-005-0642) [58] I4/mmm space group, while other were attributed to the cubic In_2O_3 phase (PDF No 01-071-2194) [57]. It is worth to mention that except the substrate diffraction peaks; no other impurity peak was identified. These observations indicate that triphenylphosphine sulfide could be a successful precursor for the growth of pure $\beta\text{-In}_2\text{S}_3$ phase at 300 and 400 °C onto glass and silicon substrates by means of a CVD process.

Considering the obtained results, it is clear that regardless the substrate type, $\beta\text{-In}_2\text{S}_3$ phase was formed at 300 and 400°C and an oxide phase was formed at 500°C; however, the phase formed at 200°C change with changing the substrate type. This can indicate that the substrate type influences mainly the starting growth of the obtained films. In fact, the absence of any phase at 200°C onto glass substrate may be attributed to lack in growth time with this condition. It is well possible also that the related peaks were too weak and therefore masked by the glass amorphous texture. For the film deposited onto silicon at 200°C, the obtained diffractogram shows that Indium exist, which means that the 100 nm of Indium might ~~be~~ not have completely reacted with S, probably due to the slower diffusion of S at this lower temperature. What is more, 200°C is not enough high temperature to transform all the indium into In_2S_3 phase. A plausible explanation for the In_2O_3 formation onto silicon substrate at 200 °C is that the substrate surface itself contains some quantity of oxygen, which reacts with the indium layer forming an oxide phase.

At 500 °C, films were formed by only In_2O_3 phase and no existence to any indium sulfide, neither metallic indium phase. This observation indicates that the sulfur atoms were snatched from the film when the temperature was raised to 500 °C, being replaced by oxygen atoms, which allows the formation of the identified oxide phase.

As the tetragonal $\beta\text{-In}_2\text{S}_3$ phase, is the main phase obtained in this study, an overview of its structure is required. In fact, $\beta\text{-In}_2\text{S}_3$ phase crystalizes in Tetragonal structure with I41/amd (D_{4h}) space group and with the following lattice parameters, $a=b=7.619 \text{ \AA}$ and $c=32.329 \text{ \AA}$. It was described as three spinel-like structure heap up along c axis where the Indium atoms occupied both octahedral and tetrahedral sites according to the following formula: $[\text{In}_6]_{\text{Oh}}[\text{In}_2\Box]_{\text{Td}}\text{S}_{12}$, where \Box indicates vacancies sites [40, 59]. With electronic configurations of In: $[\text{Kr}] 4d^{10} 5s^2 5p^1$ and S: $[\text{Ne}] 3s^2 3p^4$, $\beta\text{-In}_2\text{S}_3$ system was formed by six Wyckoff positions:

In1 (8c), In2 (16h), In3 (8e), S1 (16h), S2 (16h), and S3 (16h) with the following multiplicity 6, 6, 4, 4, 3, and 4 [60]. The schematic structure of β - In_2S_3 is shown in Figure 2.

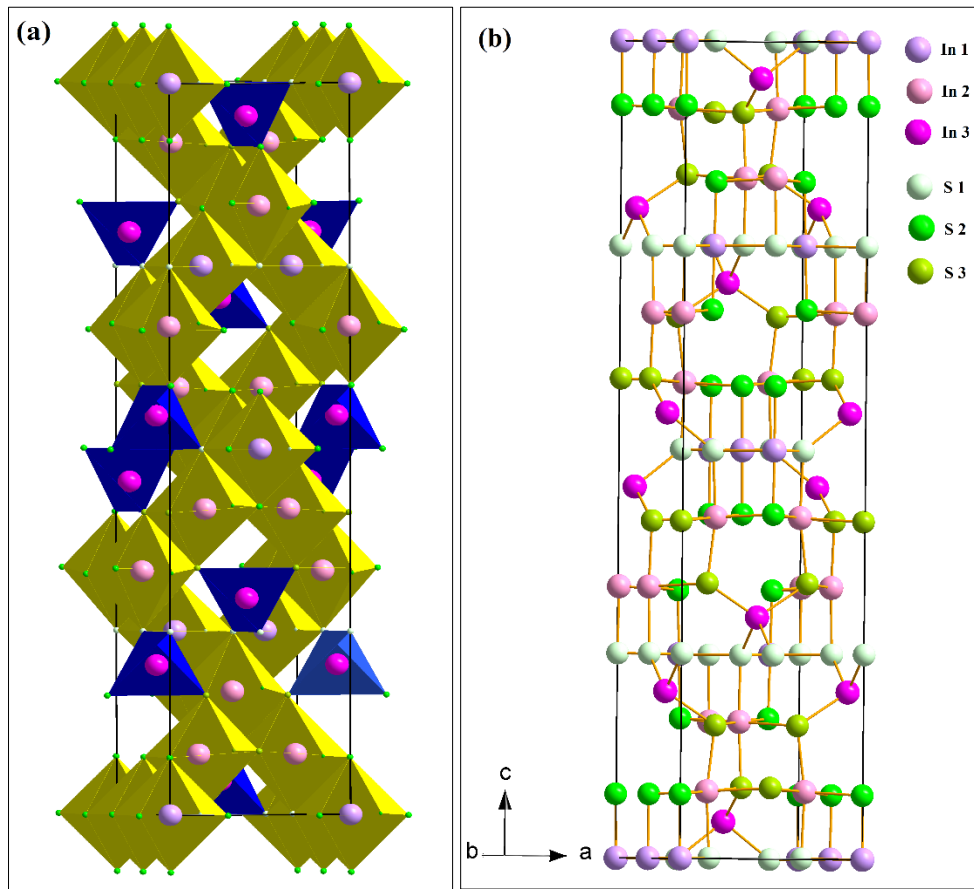


Figure 2. Perspective view of β - In_2S_3 crystal structure: (a) Polyhedron model, (b) Ball-and-stick model.

This structure was characterized also by the absence of 00l reflections and non-occupied interstices sites in the complete spinel [59].

Further information about the quality of our films can be obtained by determination of microstructure parameters. The texture coefficient, the average crystallite size (D), the dislocation density (δ) and the microstrain (ϵ) were determined using the Scherrer Formula [61] and Williamson & Smallman relations [62, 63]:

$$TC_{(hkl)} = \frac{\frac{I(hkl)}{I_0(hkl)}}{N^{-1} \sum \frac{I(hkl)}{I_0(hkl)}} \quad (8)$$

$$D = \frac{k\lambda}{\beta \cos(\theta)}; \langle D_a \rangle = \frac{\sum TC_{(hkl)} D_{(hkl)}}{\sum TC_{(hkl)}} \quad (9)$$

$$\delta = \frac{1}{D^2}; \langle \delta_a \rangle = \frac{\sum TC_{(hkl)} \delta_{(hkl)}}{\sum TC_{(hkl)}} \quad (10)$$

$$\varepsilon = \frac{\beta}{4 \tan \theta}; \langle \varepsilon_a \rangle = \frac{\sum TC_{(hkl)} \varepsilon_{(hkl)}}{\sum TC_{(hkl)}} \quad (11)$$

Where $TC_{(hkl)}$ is the texture coefficient, $I(hkl)$ is the peak intensity in the experimental spectrum, $I_0(hkl)$ is the peak intensity in the JCPDS file, N is the total reflection peaks, k is the Scherrer constant, λ is the wavelength of X-ray radiation (Cu K_α), β is the full width at half-maximum (FWHM) and θ is the diffraction Bragg angle in radian.

To evaluate deeply the effect of growth temperature and substrate type, the obtained results of the pure β - In_2S_3 films obtained at 300 and 400 °C are summarized in Table 1, while Table 2 contains the results of the pure In_2O_3 films obtained at 500 °C.

Table 1. Average grain size $\langle D_a \rangle$, dislocation density $\langle \delta_a \rangle$ and microstrain values $\langle \varepsilon_a \rangle$ of Indium sulfide (β - In_2S_3) thin films as a function of substrate type and growth temperature.

Substrate	Temperature (°C)	$\langle D_a \rangle$ (nm)	$\langle \delta_a \rangle$ ($10^{14}m^2$)	$\langle \varepsilon_a \rangle$ (10^{-3})
Glass	300	32.547	9.57	3.56
	400	37.154	11.98	3.33
Silicon	300	33.101	12.42	3.76
	400	39.221	6.77	2.88

Table 2. Average grain size $\langle D_a \rangle$, dislocation density $\langle \delta_a \rangle$ and microstrain values $\langle \varepsilon_a \rangle$ of Indium oxide (In_2O_3) thin films as a function of substrate type.

Substrate	Temperature (°C)	$\langle D_a \rangle$ (nm)	$\langle \delta_a \rangle$ ($10^{14}m^2$)	$\langle \varepsilon_a \rangle$ (10^{-3})
Glass	500	32.999	9.57	3.89
Silicon	500	45.730	5.59	2.33

Depending on substrate type and growth temperature, the crystallite size values range between 32.547 to 45.730 nm indicating the nanocrystalline quality of the obtained films. By comparison, it was noted that the crystallite size increases with increasing the growth

temperature. The slightly higher values of grain size observed for indium sulfide films deposited onto silicon substrate suggest that this type of substrate facilitates the growth of the crystallite, although the differences are not significant. Regarding to the grain size of the indium oxide obtained at 500 °C, it is also larger when the film was deposited onto silicon substrate, with higher differences, indicating that the silicon substrate allows the grains to grow faster than glass substrates. We believe that physical properties of the substrate such as thermal conductivity, specific heat, surface energy, the hydrophilicity and linear thermal expansion have an important effect on the film growth in this case [64] [65].

It is known that the dislocation density is often related to the crystal imperfection; however, the microstrain includes defaults in several forms as stacking faults, contact stress, coherency stress, triple junction... Thus, the estimation of dislocation density and microstrain can offer qualitative information about thin films.

The higher δ value was observed for the film deposited onto silicon substrate at 300 °C. This finding may be of interest as it suggests the use of this film as a sensitivity device material. For the others samples, the temperature effects on both parameters was found to be marginal and not easy to discuss.

The strain and dislocation density of the indium oxide films are lower when silicon was used as a substrate and higher in the case of glass substrate. The lower value of microstrain values can be attributed to a decrease in inter-planar atoms spacing [66]. This defect can influence certainly the optical properties that will be investigated in the following part.

The lattice parameter and inter-planer distance of indium sulfide and indium oxide films with respect to the preferential orientation were calculated and presented in Table 3 and 4 respectively.

Table 3. Lattice parameter and inter-planer distance of Indium sulfide (β - In_2S_3) thin films as a function of substrate type and growth temperature.

Substrate	Temperature (°C)	a (Å)	c (Å)	d_{109} (Å)
Glass	300	7.667	31.406	3.245
	400	7.560	31.212	3.252
Silicon	300	7.620	32.301	3.245
	400	7.609	32.376	3.248

Table 4. Lattice parameter and inter-planer distance of Indium oxide (In_2O_3) thin films as a function of substrate type.

Substrate	Temperature ($^{\circ}\text{C}$)	a (\AA)	d_{222} (\AA)
Glass	500	10.153	2.931
Silicon	500	10.167	2.935

The lattice constants (a and c) of pure $\beta\text{-In}_2\text{S}_3$ deposited on different substrates are found in the range of 7.560-7.667 \AA and 31.212-31.406 \AA respectively, which is in agreement with the values of the standard JCPDS results. The inter-plane spacing is in the range between 3.245 and 3.252 \AA , which also agree with the standard JCPDS results (3.249 \AA).

For indium oxide films, the values for the lattice parameter (a) are 10.153 and 10.167 \AA , while the values for inter-planar spacing (d_{222}) are 2.931 and 2.935 \AA for films deposited onto glass and silicon substrates respectively. These values are also in well agreement with standard JCPDS file.

3.2. Morphological study

SEM analysis is an extended technique used to study the surface morphology of the obtained thin films materials. Thus, the morphology of our films was examined by ESEM microscopy. The obtained micrographs with 10000x magnification were presented in Figure 3.

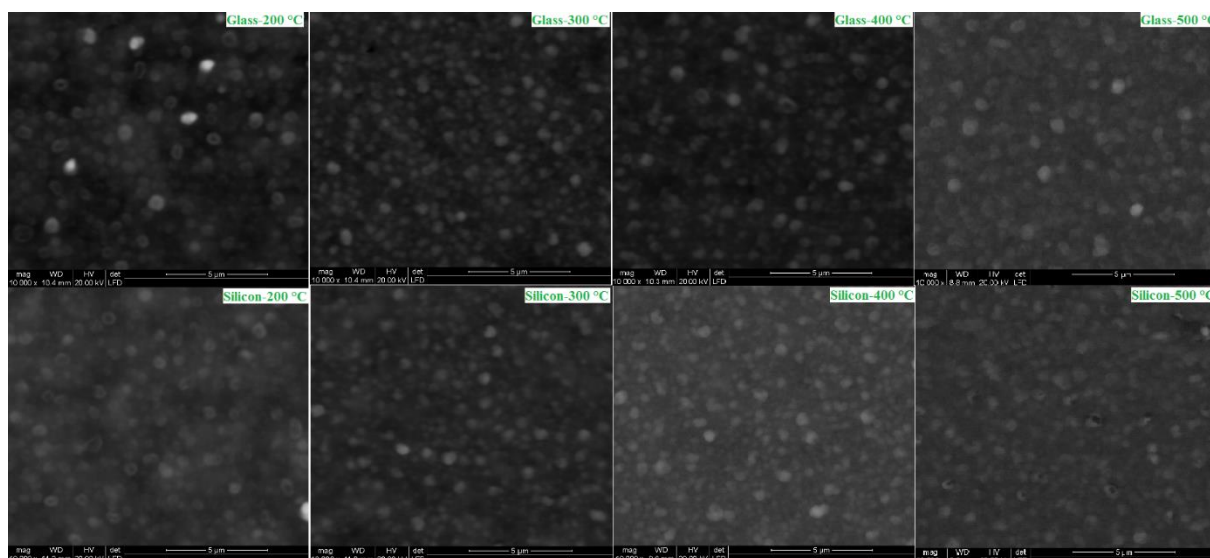


Figure 3. SEM micrographs with 10000x magnification of films obtained onto glass and silicon substrates at different growth temperatures.

From Figure 3, it is clearly observed that highly adherent and uniform films were obtained regardless the growth temperature and substrate nature. At a first glance, the micrographs of films deposited onto glass and silicon substrates are similar. For all growth temperature range, surfaces were formed by small spherical shaped grains. It is also clear that all the films are homogenous and cover completely the total substrate surface with no pinholes or cracks. It is also interesting to note that both indium sulfide films and indium oxide films have the same morphology. Note also that growth temperature and substrate nature have no remarkable effects on the surface morphology of our films.

3.3. Electronic structure and Optical related parameters

Optical studies of semiconductor materials gives important information about the band structure, which determines their useful applications. In this part, the most substantial optical parameters such as absorption coefficient, energy band gap, refractive index, extinction coefficient, dielectric parameters and optical conductivity of our samples were investigated experimentally and theoretical. For this purpose, Transmittance and reflectance measurements were recorded to ensure the determination of the experimental above-mentioned parameters, while a theoretical study was performed to determine the band structure, thereafter the determination of the dielectric functions that allows the calculation of other optical parameters.

Transmittance and reflectance

Transmittance and reflectance curves of the films were determined and shown in Figure 4.

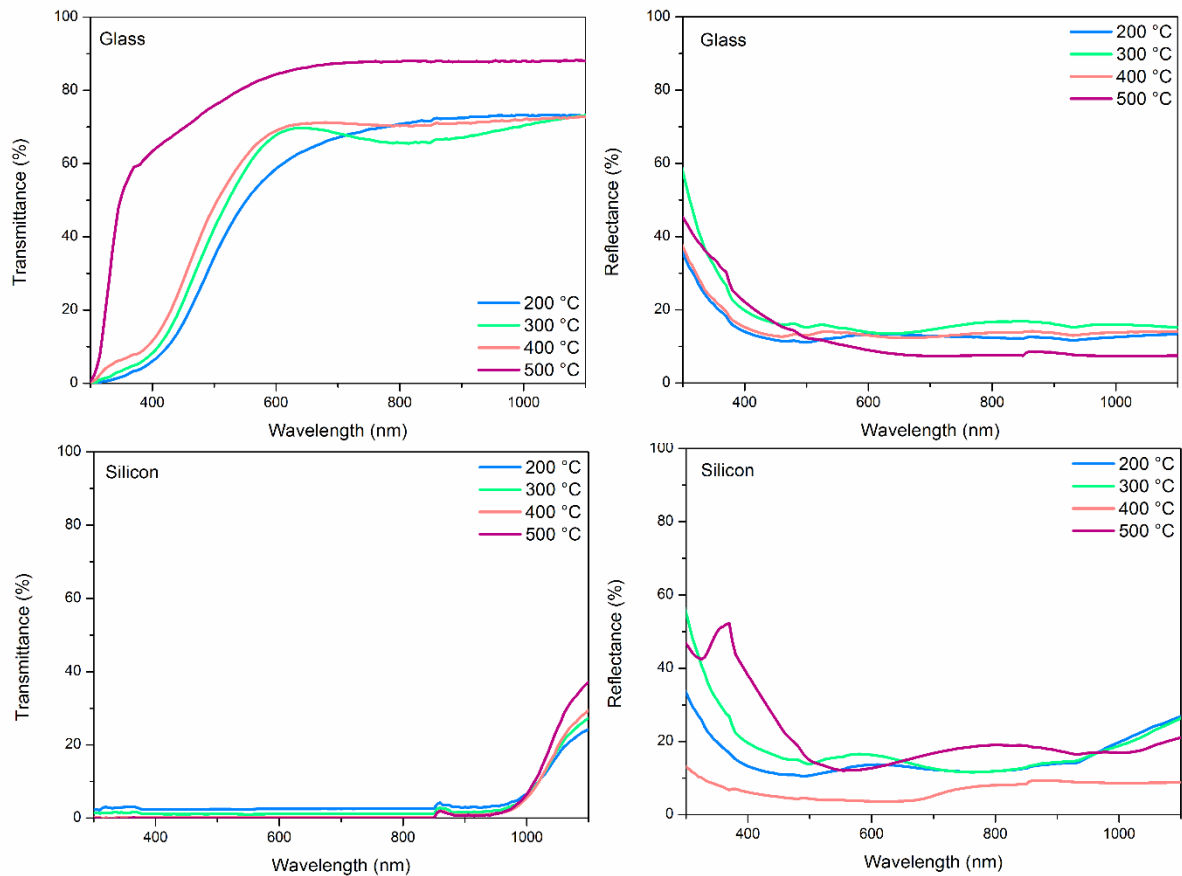


Figure 4. Transmittance and reflectance curves of the films deposited onto glass and silicon substrates at different temperature.

Indium sulfide film has a yellow color and the intensity of this color changes with changing the growth temperature, becoming white for indium oxide films. This fact will affect certainly the transmittance and reflectance properties of the obtained films. Regarding Figure 4, all indium sulfide films deposited onto glass substrates exhibit similar curve trend. They show a jump in transmittance values in the range of 350-450 nm, reaching a plateau for higher wavelengths where the transmittance values are in the range from 65% to 75%. These values are quite stable for a wide wavelength range extending from visible to IR range. These results indicate an excellent transparency and, therefore, the formation of high quality films that can be suitable as an optical window for photovoltaic structures. The interferences observed for all the films confirm their homogeneity and smoothly nature [67, 68]. The film deposited onto glass substrate at 300°C reaches the maximum value (75%) and presents higher interferences, confirming a better homogeneity. Differently to those films, indium oxide film has a different

behavior with higher transmittance, which reach 90% in Visible-IR region, indicating the higher transparency of this film.

Reflectance behavior is also similar for all the indium sulfide films and quite lower for the In_2O_3 film deposited at 500°C . Indium sulfide films show higher reflectance values in the UV region, while beyond this region decreases drastically until stabilizing around 15%. In the case of In_2O_3 the reflectance reaches a 7% in the IR region.

Comparing the spectra depicted in Figure 4, the effect of substrate nature on the films transmittance and reflectance was well remarkable. Very low transmittance in the range of UV-Visible-near IR, which does not exceed the 4%, can be noted for the films deposited onto silicon substrates. The low transparency of silicon wafer can be the origin of these lower values. This fact is well consistent with our previous results for tin selenide thin films deposited onto the same type of substrate. The jump in transmittance values in this case is observed around 1000 nm. For higher wavelengths, the transmittance values continue to increase slowly, reaching the maximum at higher wavelength. In addition, we can note that in this range, the transmittance values increase with increasing growth temperature, **except for the Indium oxide layer (obtained at 500°C)** which may be due to a decrease in surface roughness and/or a decrease in carrier concentration. Note also that the jump in transmittance of indium oxide was higher than those of indium sulfide. Similar observation was done by Ji et al. for In_2S_3 thin films deposited by RF sputtering [69]. Authors have explained the decrease in transmittance of the layers by an enhanced of surface roughness. Beena et al. also related the increase in In_2O_3 films transmittance with growth temperature to the smooth surface feature [70]. The film obtained at the lowest temperature, which contains some metallic indium, has the lowest transmittance values, however, the transmittance of films formed by pure indium sulfide phase were slightly higher. The small difference observed in transmittance of films deposited at 300 and 400°C onto silicon substrates can be attributed to the films crystallinity. Revathi et al. shows that the optical transmittance of In_2S_3 films deposited onto glass substrate was influenced by the substrate temperature, mainly in Visible region [71]. Authors explain this fact by the decrease of the number of defects with increasing temperature, which match well with our results, except for films deposited onto glass substrate at 400°C . Reflectance values of films deposited onto silicon substrates were higher than those of films deposited onto glass substrates, which was expected due to the opacity of silicon substrate. Note also that the film deposited onto silicon substrate at 400°C shows the lower reflectance value; this

can be attributed to their lowest microstrain and dislocation density values compared to other films. Others factors such as crystallinity state, homogeneity, microstructure, thickness, grain size... can be also the origin of the differences observed.

Absorption coefficient

The experimental absorption coefficient was calculated using the transmittance (T) and reflectance (R) data, based to the following relation, where d is the film thickness. The results are shown in Figure 5.

$$\alpha = \frac{1}{d} \ln \frac{(1 - R)^2}{T} \quad (12)$$

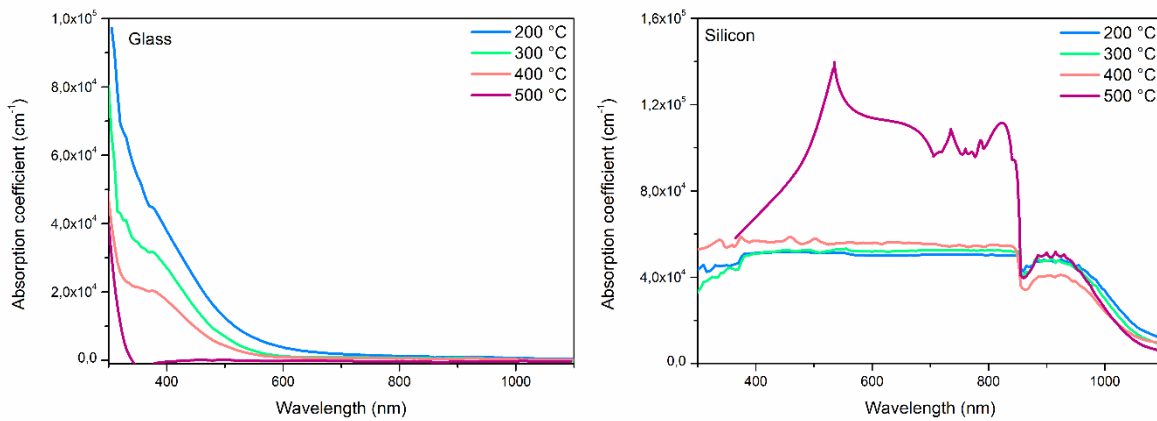


Figure 5. Optical absorption coefficient versus wavelength for Indium sulfide thin films deposited onto glass and silicon substrates at different temperature.

As shown, all films show high optical absorption coefficient (in the range of 10^4 cm^{-1}) independently of the substrate type and growth temperature. For indium sulfide films deposited onto glass substrates, the effect of growth temperature is well remarkable, although for all of them the absorption coefficient reaches the maximum value for the lower wavelengths values (a quite narrow range), decreasing drastically to reach almost a zero value for wavelengths over 700 nm. In fact, the amorphous film obtained at 200 °C has the higher absorption coefficient despite no phase was identified. When increasing the growth temperature to 300°C and 400°C, α has a lower value, but it is still in the range of 10^4 cm^{-1} . Finally, indium oxide film shows a different behavior, in fact, α decreases drastically reaching the minimum at 350 nm.

Indium sulfide films deposited onto silicon substrates also show an absorption coefficient in the order of 10^4 cm^{-1} , but for larger wavelength range, that extends from UV to near IR region, which can be attributed to the silicon substrate effect. For the indium oxide film a higher absorption coefficient in the order of 10^5 cm^{-1} was observed in the same range from visible-near IR, following the same behavior of the other layers for higher wavelengths. The high optical absorption coefficient of our films suggest their useful application as photo material. In order to confirm this result, the theoretical optical absorption coefficient $\alpha(\omega)$ was calculated using relation (4) based on single crystal data of $\beta\text{-In}_2\text{S}_3$. Figure 6 show the theoretical optical absorption spectrum of $\beta\text{-In}_2\text{S}_3$ in the range of 300-1100 nm.

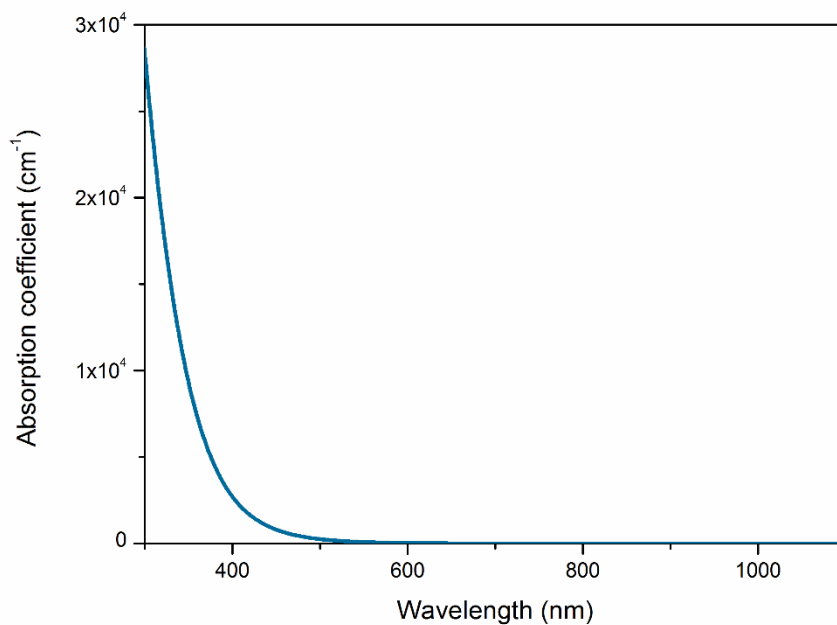


Figure 6. The theoretical optical absorption coefficient spectrum of $\beta\text{-In}_2\text{S}_3$.

As shown, the theoretical absorption coefficient of the single crystal $\beta\text{-In}_2\text{S}_3$ is in the range of 10^4 cm^{-1} , which is in good qualitative agreement with the experimental measurement. The same behavior obtained for the experimental α spectrum of pure $\beta\text{-In}_2\text{S}_3$ thin films deposited onto glass substrates can be also noted. However, the behavior was dissimilar to $\beta\text{-In}_2\text{S}_3$ thin films deposited onto silicon substrates, which is expected taking into account the substrate effects demonstrated in the previous section.

Electronic structure and Energy band gap

$\beta\text{-In}_2\text{S}_3$ presents a controversy about the type of electron transition from valence to conduction band. Several authors treat it as direct allowed transition [20, 72] while few

publications consider it an indirect allowed transition [73]. Some others treat it as a direct forbidden transition [74]. In our case and for all obtained samples, $(\alpha h\nu)^n$ were plotted against $h\nu$, based on the following Tauc plot relation:

$$(\alpha h\nu)^n = A(h\nu - E_g) \quad (13)$$

In our case, for all films characterized the best straight lines were obtained when $n=2$. Figure 7 show the plot of $(\alpha h\nu)^2$ versus $h\nu$ of films deposited at different temperatures onto glass substrates.

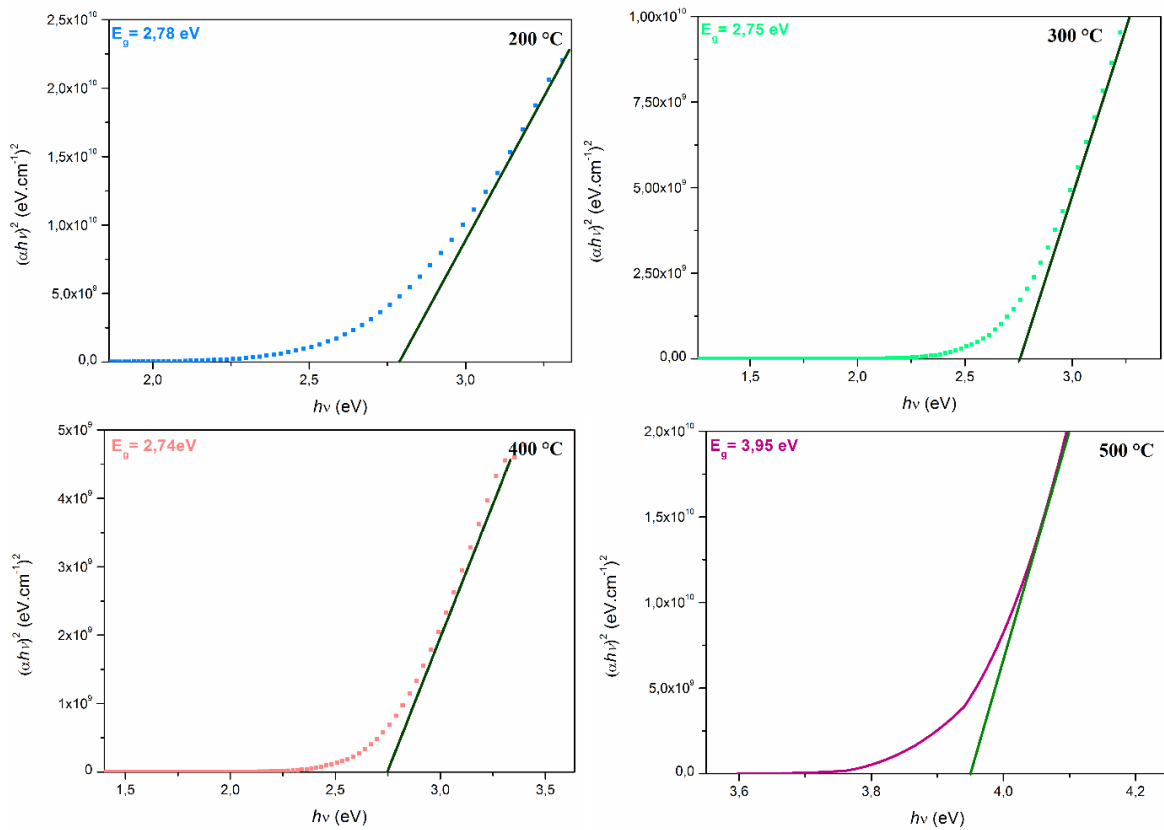


Figure 7. $(\alpha h\nu)^2$ versus photon energy for films deposited onto glass substrates at different temperatures.

From the obtained plots, it seems that all films show direct allowed transition. The energy band gap obtained for β -indium sulfide films grown onto glass substrates was found to be in the order of 2.7 eV, that matched well with the bibliographic data [32, 75]. Note that the band gap values of the pure indium sulfide films obtained at 300 and 400 °C were found to be so closer. Indium oxide thin film deposited onto glass substrate has a direct band gap $E_g = 3.95 \text{ eV}$ which is higher than the value mentioned by Chong et al. (2.9 to 3.1 eV) [76] and closer to the

values obtained by Naseem et al. ($E_g=3.92$ eV) for indium oxide films obtained by evaporation of indium in the presence of oxygen [77].

As a matter of fact, the bibliographic data presents an ambiguity about the band gap nature of $\beta\text{-In}_2\text{S}_3$. This can be certainly due to the interactions of each atom with their neighbors, which affect crucially the band structure of the indium sulfide, thus their band-edge. In fact, some numerical approaches have shown that the p orbitals of sulfur atoms are mainly located in the top of valence band (VB) [23]. Thereafter, excess or defaults in sulfur atoms can affect highly the band gap width.

Thereby, in order to get further insight about the type of electrons transition between valence band and conduction band of $\beta\text{-In}_2\text{S}_3$, we have computed here their electronic band structure in order to clarify the chemical bonding interactions. For this purpose, an optimization of the atomistic structure was carried out firstly using DFT in order to get local minima within the DFT. Thus, the band structure of $\beta\text{-In}_2\text{S}_3$ along the high symmetry lines in the irreducible Brillouin zone is plotted from -3.0 to +5.0 eV in Figure 8.

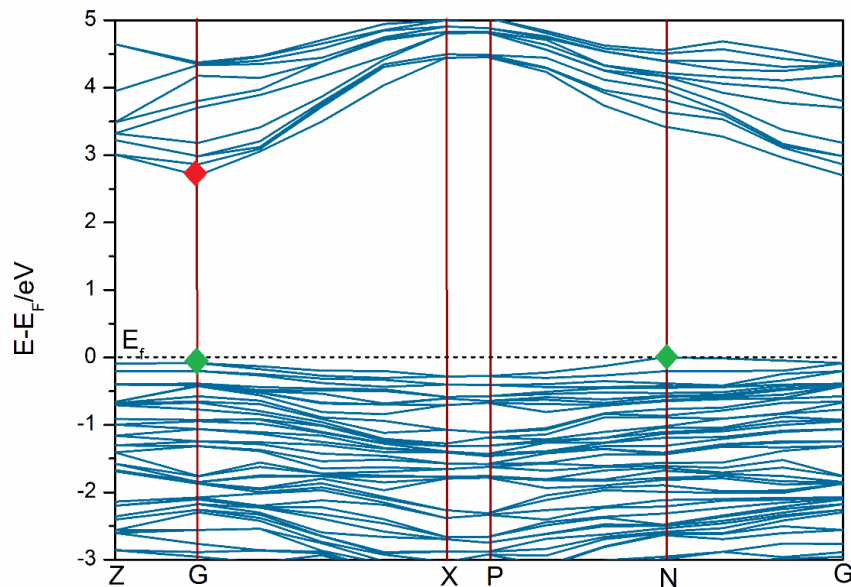


Figure 8. The calculated band structure of $\beta\text{-In}_2\text{S}_3$ single crystal.

As shown, the Fermi level was regarded as 0 eV and is marked by a horizontal dotted line. This level correspond also to the top of the valence band. It is clearly observed that the conduction band minimum was located at G point (2.72 eV), while the valence band maximum was found away G point (-0.06 eV) and was located at N point (0 eV). This finding indicate that $\beta\text{-In}_2\text{S}_3$ has

an indirect band gap. Regarding to the low difference in energy between the points G and N (0.06 eV in our case), some researchers considered that $\beta\text{-In}_2\text{S}_3$ has a direct band gap transition. These multiple optical transitions make this material a promising candidate for optoelectronic applications.

Based on this, a direct band gap can be considered in G point with energy of 2.66 eV. This value agrees well with our experimental result for the direct band gap value of the pure $\beta\text{-In}_2\text{S}_3$ around 2.7 eV. The difference between the theoretical and experiments values can be attributed to the quantum size of the films.

Density of states

In order to get a deeper understanding about the origin of $\beta\text{-In}_2\text{S}_3$ optical properties and to specifies the composition of each band, a numerical approach was performed by ab initio density-functional theory (DFT), using the plane-wave pseudo-potential method. The calculated partial density of states (PDOS) and total density of states (TDOS) of $\beta\text{-In}_2\text{S}_3$ are plotted in Figure 9 and 10 respectively. Fermi level was also taken as zero energy.

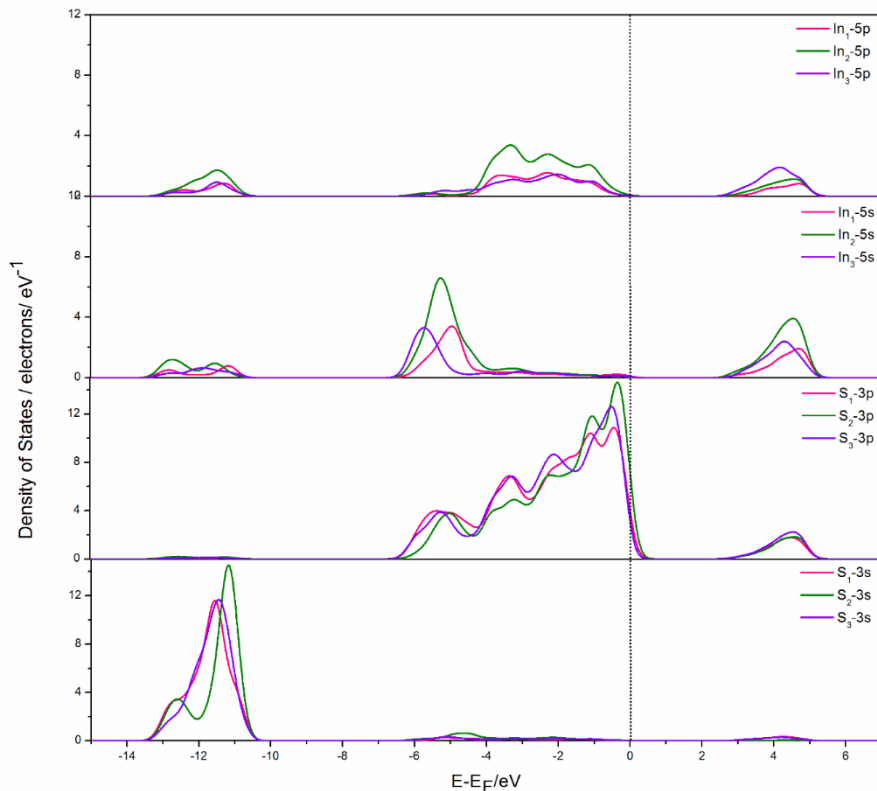


Figure 9. Partial density of states (PDOS) of $\beta\text{-In}_2\text{S}_3$ single crystal.

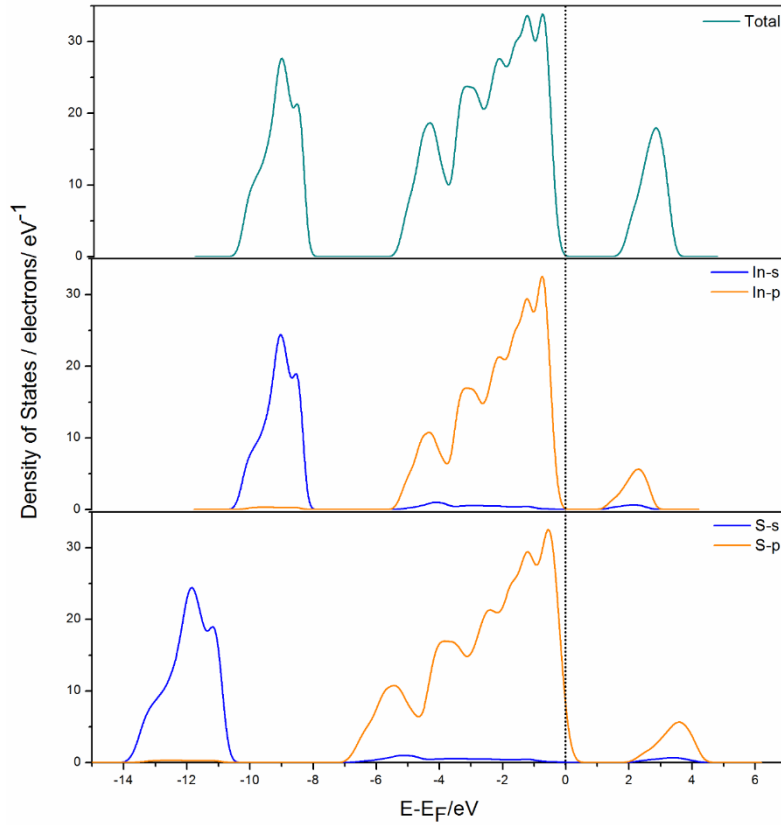


Figure 10. Total density of states (TDOS) of β - In_2S_3

The calculated DOS shows that conduction band (CB) and valence band (VB) are mainly composed by S-3s, S-3p, In-5s and In-5p states. It is clear also that In-5d states do not appear in any band, because they are completely filled with electrons. The valence band (VB) was mainly composed by two parts. The first one, centered at -10.4 eV, has a bandwidth of 3.6 eV and it is formed mainly by S-3s states. However, the hybridization between S-3p and In-5s, 5p states yield to the appearance of the second broad part at -3.67 eV, with a bandwidth of 6.65 eV. The conduction band (CB) starts around 2.6 eV with a bandwidth of 2.8 eV. This region was composed by S-3p states, In-5s states and In-5p states.

Extinction coefficient and refractive index

Extinction coefficient (k) and refractive index (n) are considered among the important parameters of optoelectronic devices that allows collecting information about the local field and the ions electronic polarizability. Hence, using the results obtained for the absorption coefficient (α) and the reflectance (R) for each wavelength (λ), we have determined the experimental n and k parameters based to the following relations:

$$k = \frac{\alpha\lambda}{4\pi} \quad (14)$$

$$n = \frac{1 + R}{1 - R} + \sqrt{\frac{4R}{(1 - R)^2} - k^2} \quad (15)$$

The variation of both parameters (k and n) were plotted as a function of wavelength and presented in Figure 11 for films deposited onto glass and silicon substrates.

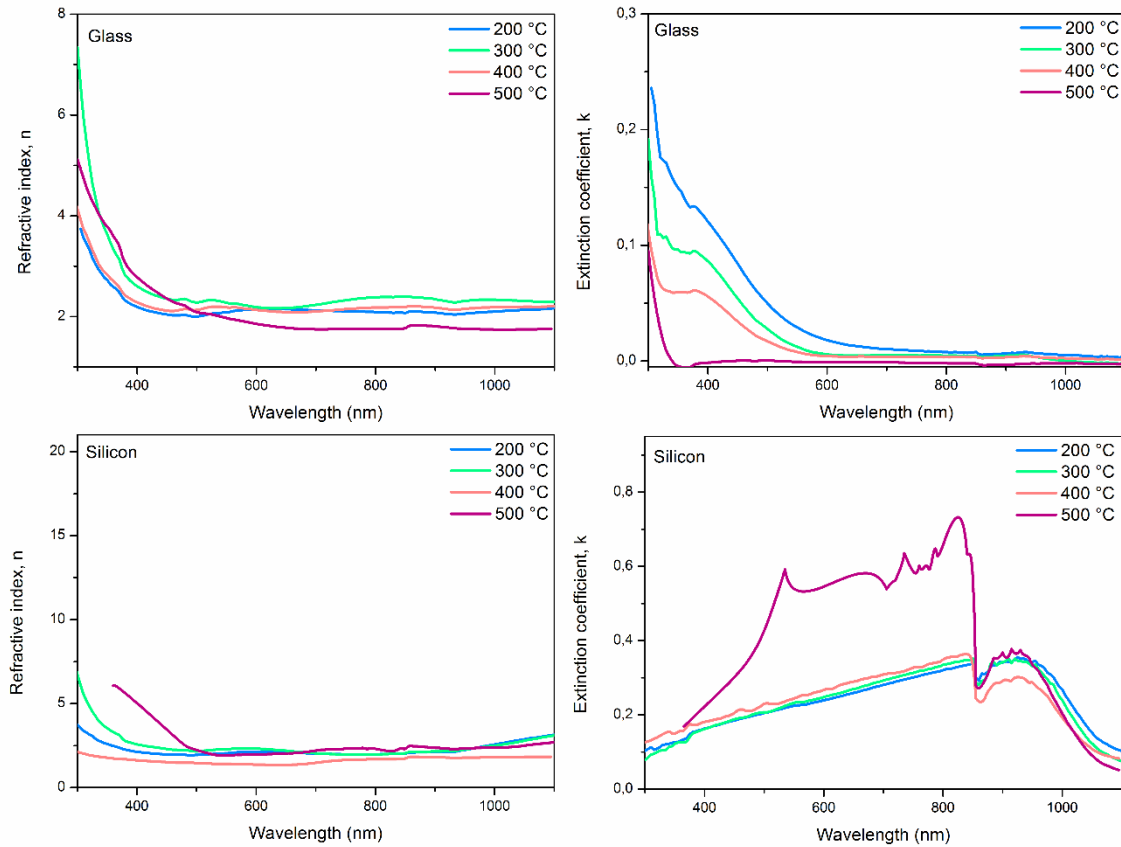


Figure 11. Refractive index and Extinction coefficient of the films deposited onto glass and silicon substrates at different temperatures.

It is clearly visible from Figure 11 that the maximum extinction coefficient values of the indium sulfide films deposited onto glass substrates were found in the range of 0.19-0.24 in UV region. These values decrease continuously with increasing wavelength until reaching the minimum values (≈ 0) in IR region. This observation indicates that all films are transparent in this region, which matched well with the transmittance spectra analysis. Ji et al. have observed similar trends for indium sulfide thin films deposited by RF magnetron sputtering and related the zero value of k to the transport feature of indium sulfide material [34]. It must also be noted that

a little bit change can be observed as a function of growth temperature. In fact, in lower wavelength range it is noted that k values decrease with increasing growth temperature. For indium oxide film, the behavior was slightly different as the decrease of k was found to be faster and the zero value was reached in UV region, which indicate the high smoothness of this film.

Figure 11 shows that films grown onto silicon substrates have an opposite k behavior compared to films obtained onto glass substrates. K values of β - In_2S_3 films increase slightly until reaching the maximum (≈ 0.35) at 900 nm, after that the values return to decrease until reaching the lower values (0-0.1). It is obvious that films deposited onto silicon substrates have higher k values for all the wavelength range, which revealed the lower transparency of these films compared to those films grown onto glass substrates, as one could expect due to the silicon substrate influence.

A typical dispersion behavior of refractive index can be noted. It decreases drastically with increasing wavelength until becoming fairly constant at IR region. The refractive index of indium sulfide films deposited onto glass substrates varied in the range of 1.9-2.4 when the wavelength is larger than 400 nm. This observation was found to be similar to those observed by Rasool et al. [50] and Revathi et al. [78]. One can notice that the amorphous film obtained at 200°C has the lower n value, which may be attributed to their poor crystallinity, thus, to the lower packing density of this film. This parameter value was found to be slightly higher when films were grown onto silicon substrates, which indicates the suitable application of these films as optical waveguide. This observation is in accordance with the silicon substrates nature. In fact, silicon was known by its opacity in the visible region and by its transparency in IR portion of spectrum. This is why the difference in n values of indium sulfide films deposited in both substrates was remarkable in low wavelength portion, while at high wavelengths region the difference is lower. This finding confirms again the higher effect of substrate nature on optical properties. Indium oxide film grown onto glass substrate has the lowest refractive index value (≈ 1.8) which is close to those obtained by Senthilkumar et al. [79].

The theoretical refractive index (n) and extinction coefficient (k) were also computed for Indium sulfide using expressions (4) and (5).

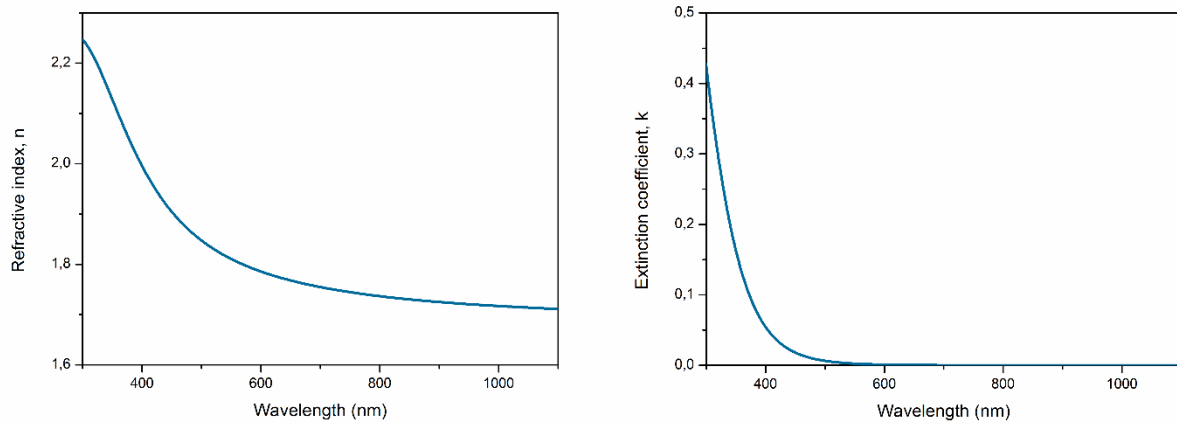


Figure 12. Calculated refractive index and extinction coefficient of β -In₂S₃.

The results are plotted in Figure 12 as a function of wavelength to allow the comparison to the values obtained from experimental measurements. The Figure shows that for the full wavelength range, the extinction coefficient has the same behavior than the absorption coefficient. It is important also to note that, for the range of 300-1100 nm, n decrease slightly with increasing wavelength, while k decrease drastically, reaching zero value around 530 nm.

Comparing these results with the experimental ones in Figure 11, similar trends can be observed. Nevertheless, n value derived from experimental measurements show a sharper decrease than the theoretical one, while k value calculated from experimental measurements reaches a zero value for higher wavelengths than the theoretical one, showing like a shoulder not present in the theoretical one.

Dielectric constant

In general, the dielectric constant of semiconductors reflects their electrical properties by measuring the interaction of electromagnetic fields with the material [80]. Using the extinction coefficient (k) and the refractive index (n), the real (ϵ_r) and imaginary (ϵ_i) part of the dielectric constant of our films were determined from the following relations:

$$\epsilon = \epsilon_r + i\epsilon_i \quad (16)$$

$$\epsilon_r = n^2 - k^2 \quad (17)$$

$$\epsilon_i = 2nk \quad (18)$$

The variation of dielectric constants (ϵ_i and ϵ_r) as a function of photon energy for films deposited onto glass and silicon substrates at different temperature was summarized in Figure 13.

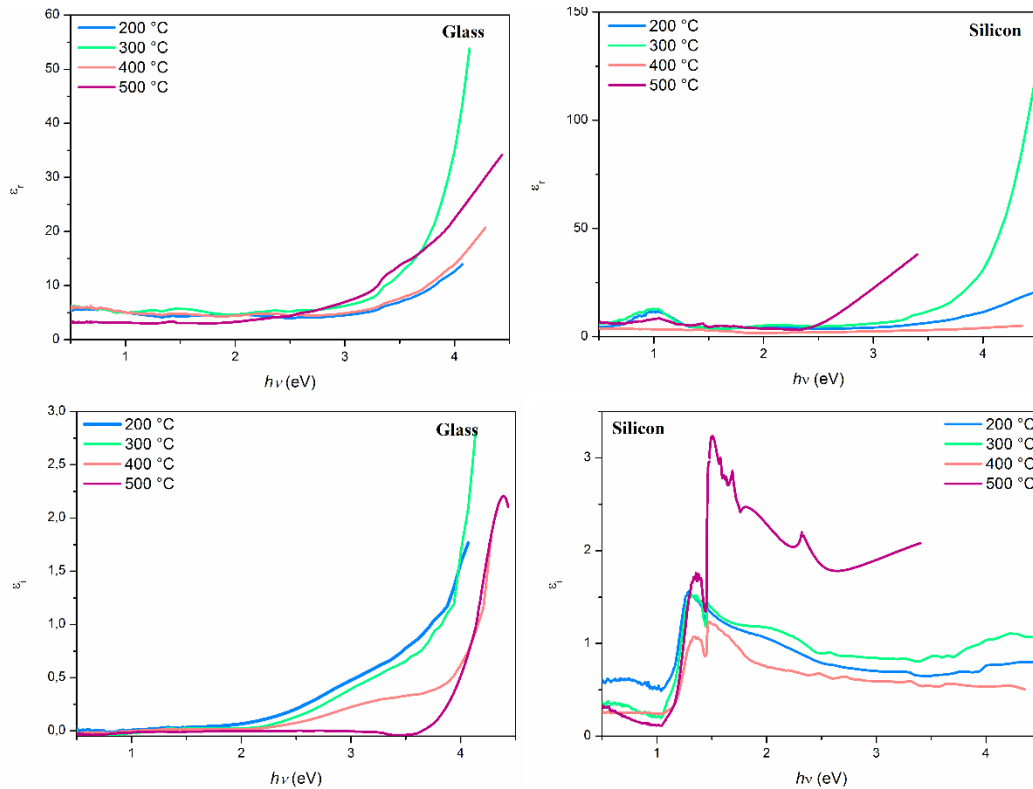


Figure 13. Dielectric constants of the films deposited onto glass and silicon substrates at different temperatures.

As expected, the real part of dielectric constant (ϵ_r) show the same variation as the refractive index (n); this is due to the lower k^2 values in comparison to n^2 values. Note that this constant was linked to the capacity of materials to store energy [81]. As shown from Figure 13, ϵ_r values increase with increasing the photon energy, which means that the amount of energy storage was higher when films were exposed to higher photon energy excitation for all the obtained films, except indium oxide film on silicon substrate, that shows a maximum value at ≈ 3.3 eV. The imaginary part (ϵ_i), named also loss factor, is a parameter that represents the loss of energy in a dielectric medium when is subjected to an external electromagnetic field [82]. Thus, indium sulfide films deposited onto glass substrates were found to be lossless in the energy range lower than 2 eV. For higher energies, the loss factor increases with $h\nu$ until reaching the maximum around 4 eV. The energy loss was higher when indium sulfide films

were grown onto silicon substrates. More peaks and bottoms can be observed for these samples, which reflect the higher interactions between photons and electrons in these films. Interestingly, for films formed by pure indium oxide phase, a quite different dielectric behavior can be observed, indicating that the dielectric properties were given by the structural properties of the material.

Concerning the difference on values of real and imaginary parts as a function of growth temperature, it is difficult to be explained, but it can be related to the absorption mechanism of energy as well as to the free phonon and electrons [83]. Thus, the present investigation of the dielectric properties of our samples indicate their useful application in capacitor design at higher photon energy range [84].

In order to confirm our finding, the experimental results were compared to the theoretical one determined using expressions (2) and (3). The calculated real and imaginary parts of the dielectric function of $\beta\text{-In}_2\text{S}_3$ are plotted in the energy range 0-14 eV in Figure 14. A magnification of the 0-4 eV region is depicted in order to allow a comparison with the values calculated from the experimental results.

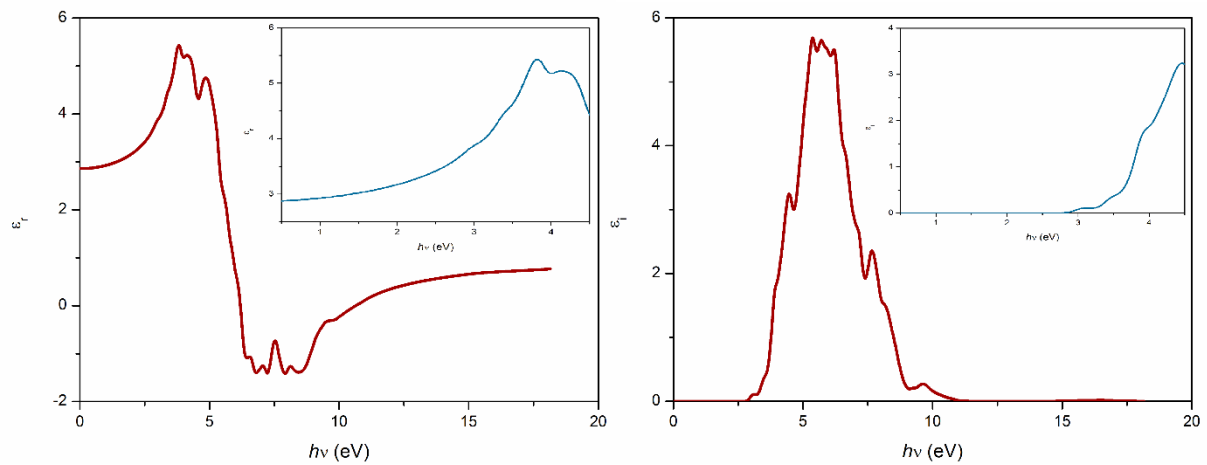


Figure 14. Calculated dielectric function of $\beta\text{-In}_2\text{S}_3$. Inset shows zoomed out region of 1-4.5 eV.

From Figure 14 it can be noted that real and imaginary parts of dielectric function present a dissimilar behavior in the full photon energy range. However, the intersection between both parts that corresponds to the gap energy transport E_t was noted in 5 eV. Focusing in the 0.5-

4.5 eV range, we can remark that both ϵ_i and ϵ_r increase with increasing photon energy which is fully consistent with our experimental observations reflected in Figure 13.

Optical conductivity

The electronic states of semiconductor materials can be studied through their optical conductivity behavior. For this reason, the optical conductivity of our samples was determined using the following relation [85]:

$$\sigma_{opt} = \frac{\alpha n c}{4\pi} \quad (19)$$

Where, α is the absorption coefficient, n is the refractive index and c is the speed of light in vacuum. Figure 15 shows the plots of optical conductivity σ_{opt} versus photon energy ($h\nu$).

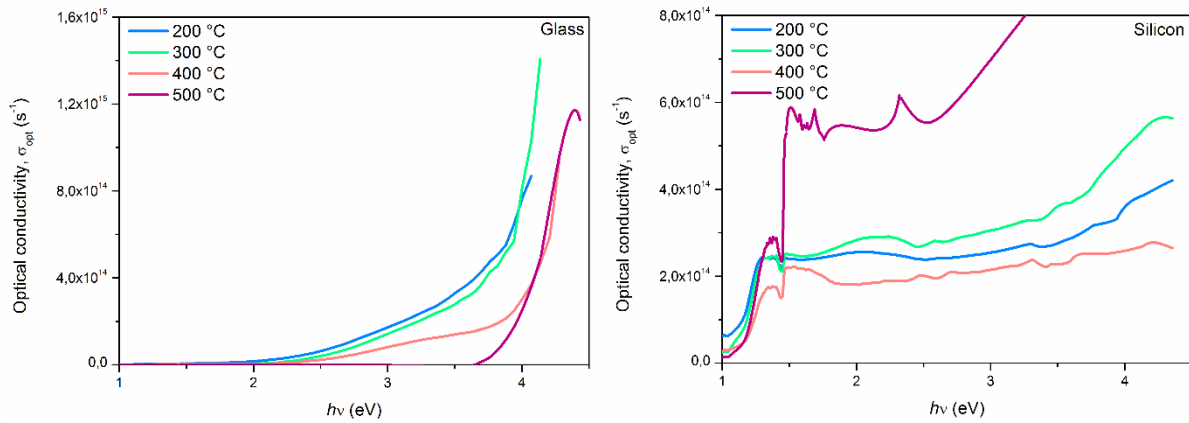


Figure 15. The plots of optical conductivity σ_{opt} against $h\nu$ of the films deposited onto glass and silicon substrates at different temperatures.

As shown from the obtained graphs, the optical conductivity of the indium sulfide films deposited onto glass substrates was very low when $h\nu < 2$ eV. Above this region, σ_{opt} starts to increase slightly until reaching their maximum around 4 eV. For indium oxide film grown onto glass substrate, the optical conductivity starts to increase when $h\nu = 3.7$ eV and reaches the maximum around 4.5 eV. The effect of temperature can be clearly observed. In fact, the more the growth temperature increases, the more the starting increase of σ_{opt} shifts toward the higher photon energy values. It can be noted also that at low temperature, films deposited

onto glass substrates shows a negligible variation of optical conductivity. This finding can be related to the absorption mechanism of energy.

The effect of substrate type on the optical conductivity of our films was remarkable. In fact, different σ_{opt} behavior was noted when films were grown onto silicon substrates. Firstly, the optical conductivity values increase promptly until 1.5 eV. Up to this range, it continues to increase slightly until reaching their maximum at higher $h\nu$ values. Note also that indium oxide film has higher σ_{opt} values compared to indium sulfide films and contrary to the one obtained onto glass substrate. The effect of temperature on the optical conductivity of films cannot be easily identified when films were grown onto silicon substrates. Thus, we can conclude that the optical conductivity was affected by the growth temperature, the film nature as well as the substrate type. Others sub-factors such as grain size, crystalline structure and the presence of oxygen sites can be in the origin of the observed difference. Further, the higher σ_{opt} values of the obtained films indicates their useful integration in optical device applications.

The theoretical optical conductivity of $\beta\text{-In}_2\text{S}_3$ computed using expression (7) was plotted in Figure 16.

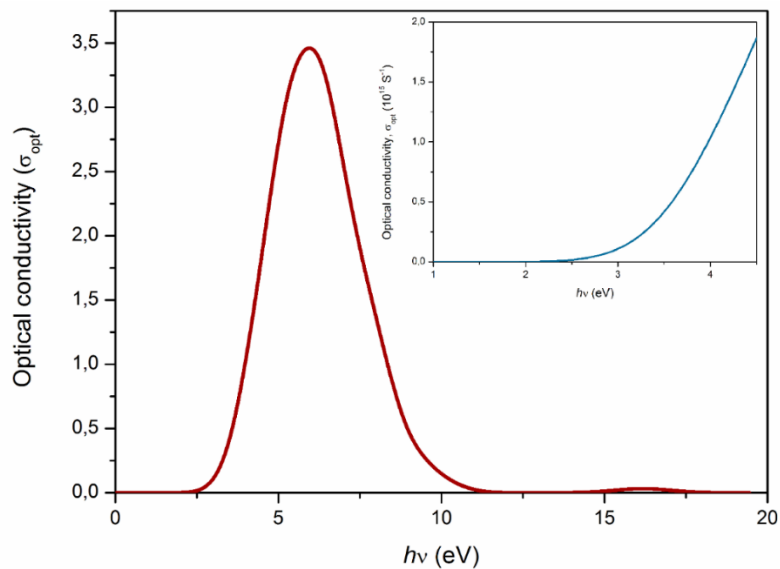


Figure 16. Calculated optical conductivity of $\beta\text{-In}_2\text{S}_3$. Inset shows zoomed out region of 1-4.5 eV.

As shown, the calculated optical conductivity increases firstly with increasing photon energy reaching a maximum of $3.47 \cdot 10^{15} \text{ S}^{-1}$ at 6 eV. Above this region, σ_{opt} falls off until reaching the

zero around 11.5 eV. Zooming to the range of 1-4.5 eV, we can note that the theoretical σ_{opt} has an identical shape to the experimental one of pure $\beta\text{-In}_2\text{S}_3$ obtained onto glass substrates.

3.4. Optical parameters

In the following, the rest of the optical parameters of the films deposited onto glass substrates were evaluated only as a function of growth temperature, since the influence of the substrate nature was clearly identified in the previous results.

Dissipation factor

Dissipation factor, called also loss tangent factor ($\tan \delta$) is also a dielectric parameter that describes the durability or/and the quality of oscillation. In other words, this parameter represents the ability of a dielectric to generate heat [86]. This parameter was defined as the ratio of the imaginary part to the real part of dielectric constants. The variation of loss factor of our samples deposited onto glass substrates was graphically presented in Figure 17.

$$\tan \delta = \frac{\varepsilon_i}{\varepsilon_r} = \frac{2nk}{n^2 - k^2} \quad (20)$$

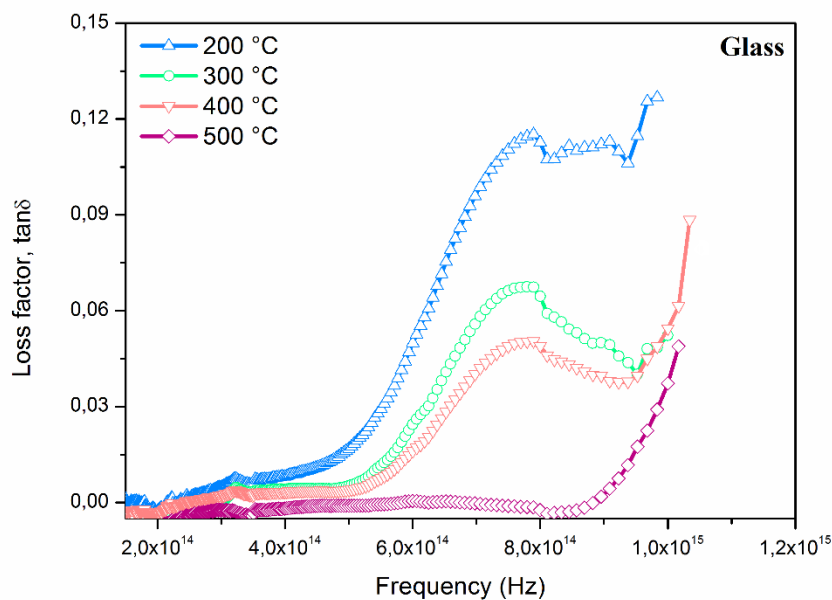


Figure 17. Loss factor of the films deposited onto glass substrates at different temperatures.

As shown, the dissipation factor for all the films obtained was quite low and for frequency higher than $3.6 \cdot 10^{14}$ Hz, $\tan \delta$ increase slowly with increasing the frequency until reaching their maximum at higher ν values. This increase in $\tan \delta$ values indicates that in these films can happen a thermal fault at higher frequency [87]. It can also easily be observed that the loss factor decreases with increasing the growth temperature, thus the indium oxide film has the lowest values of dissipation factor. Overall, the low loss values of our samples suggest their useful applications in microelectronic devices.

Oscillator and dispersion energy

Oscillator energy (E_o) and dispersion energy (E_d) are another important parameters that should be known about semiconductors materials in order to ensure the optical device modeling and design. These parameters were determined according to the concept of single-oscillator model using the following expression [88]:

$$n^2 - 1 = \frac{E_d E_o}{E_o^2 - E^2} \quad (21)$$

where n is the refractive index, E_d is the dispersion energy, E_o is the oscillator energy and E is the photon energy. According to the above-mentioned relation, the extrapolation of the linear part of $(n^2 - 1)^{-1}$ versus E^2 plot to the vertical axis, E_o/E_d can be determined, while, $E_d E_o$ values can be obtained from the slope. The plots of $(n^2 - 1)^{-1}$ versus $(h\nu)^2$ for the samples deposited onto glass substrates were illustrated in Figure 18 and the obtained E_o and E_d values were summarized in Table 5.

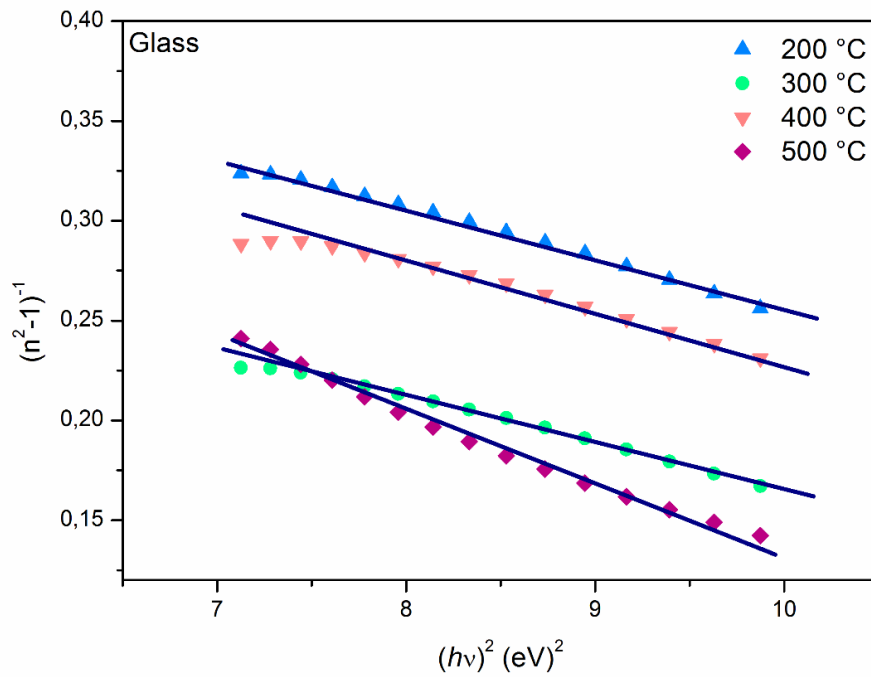


Figure 18. The plots of $(n^2-1)^{-1}$ against $(h\nu)^2$ of the films deposited onto glass substrates at different temperatures.

Table 5. The estimated E_d , E_o and E_o/E_g values of the films deposited onto glass substrate as a function of growth temperature.

Temperature (°C)	200	300	400	500
E_d (eV)	10.72	13.57	12.01	10.29
E_o (eV)	3.70	3.29	3.73	2.66
E_g (eV)	2.78	2.75	2.74	3.95
E_o/E_g	1.33	1.20	1.36	0.67

As it is well known, the dispersion energy (E_d) was considered as a potential parameter related to the distribution of charge and to the nature of chemical bonding within the unit cell of semiconductor materials. More precisely, it measures the average intensity of the optical inter-band transitions independently of the band gap [89]. Indeed, E_d parameter was closely related to the effective coordination number of atoms and valence (the effective number of valence electrons per anion and to the anion chemical valence) [88]. For our samples deposited onto glass substrates, E_d values were found to be slightly influenced by the growth temperature. In the case of pure indium sulfide films, E_d was found to be equal to 13.57 and

12.01 eV respectively. These values are in agreement with the values obtained by Timoumi et al. for indium sulfide films deposited by vacuum thermal evaporation technique [49]. Moreover, the E_d values for the no-pure phase, the indium oxide phase and the β - In_2S_3 phase are quite different. This finding confirms the dependence of this parameter on the chemical bonding, coordination number and valence.

The single oscillator (E_o) is the WDD (Wemple–DiDomenico) parameter that gives information about the average excitation energy and it depends strongly on the energy band gap. As shown, E_o is in the range of 3 eV for the pure indium sulfide films and is lower (≈ 2.5 eV) for the indium oxide film. Thereby, the effect of film nature on this parameter is remarkable. The obtained single oscillator values, as well as E_o/E_g values are close to those observed by Timoumi et al. for indium sulfide films grown by vacuum thermal evaporation method [50].

Urbach energy (Band tail width)

In general, for the semiconductor materials, two important regions can be identified in their optical absorption spectra besides to the strong absorption region, which is related to the energy gap. One weak absorption region related to defects into the film and other edge absorption region that depends on the structural perturbation and disorder into the film. Moreover, near to the optical band gap region, the absorption edge obeys to the Urbach rule according to the following relations [90]:

$$\alpha = \alpha_0 e^{\frac{hv}{E_u}} \quad (22)$$

$$\ln\alpha = \ln\alpha_0 + \frac{hv}{E_u} \quad (23)$$

where α is the absorption coefficient, α_0 is a constant, hv is the incident photon energy and E_u is the band tail width (Urbach energy) that is related to the localized states available at band edges [91].

According to the above-mentioned formula and plotting $\ln\alpha$ versus hv , the inverse of the slope of the straight-line part of the plot gives the band tail width. Figure 19 shows the plot of $\ln(\alpha)$ versus hv for the films obtained onto glass substrates. The estimated Urbach energy E_u values were summarized in Table 6.

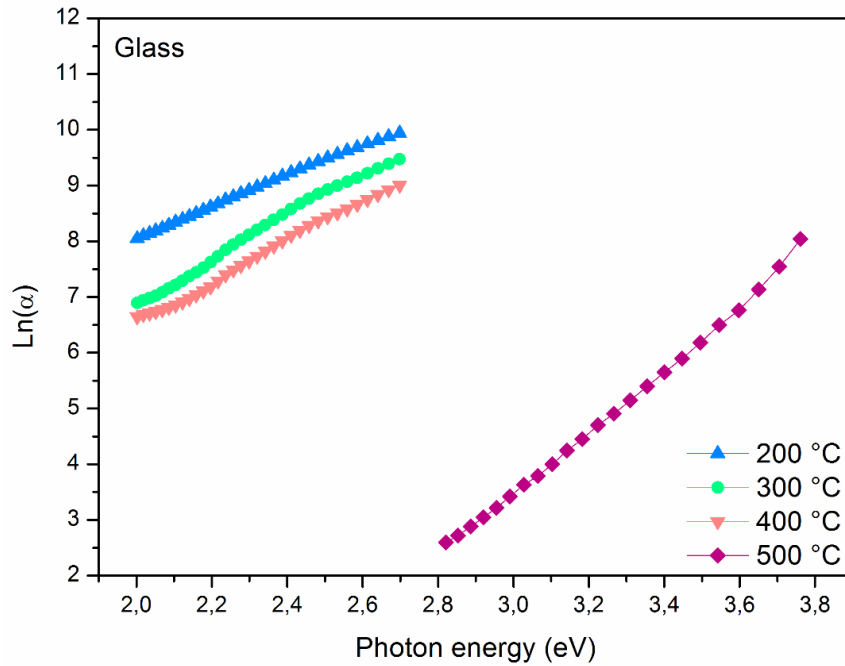


Figure 19. Plots of $\text{Ln}(\alpha)$ against $h\nu$ of the films deposited onto glass substrates at different temperatures.

Table 6. The estimated E_u values of the films deposited as a function of growth temperature.

Temperature (°C)	200	300	400	500
E_u (eV)	0.36	0.25	0.27	0.17

Considering the estimated E_u values, it is clear that the film grown onto glass substrates at 200°C has the highest Urbach's energy. This result was expected for its amorphous nature and due to its poor crystallinity compared to others films [93]. In fact, the higher E_u values matches with the creation of higher disorder, thus the formation of higher width of localized states in the band gap [94]. The lower band tail width observed for film grown at 500 °C indicates the lower number of localized states available in this film compared to others. One may notice that for both pure $\beta\text{-In}_2\text{S}_3$ films, E_u values are close. Note also that the effect of the microstrain and dislocation density on the E_u value is difficult to be identified, which suggest that Urbach energy can be probably affected by other types of defects besides the dislocation density and microstrain that have more powerful effects to the width of localized states.

3.5. PL measurements

Photoluminescence (PL) study is among the helpful tools that allows the study of semiconductors materials properties. More precisely, PL study gives information about the quality and origin of defects into the materials, such as donors, acceptors, vacancies, interstitials... Thus, photoluminescence measurements were carried out at room temperature for our films. The obtained spectra are shown in Figure 20.

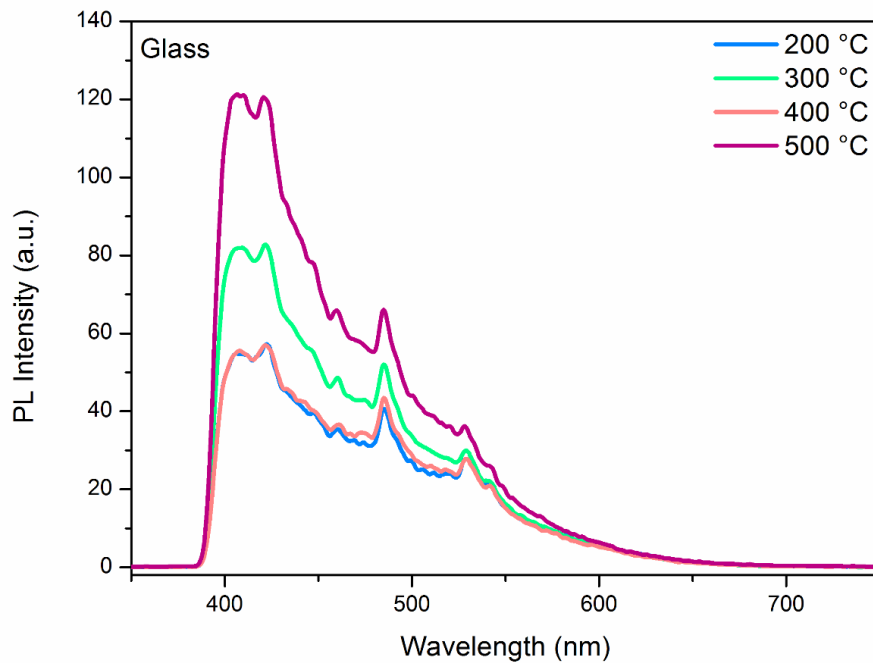


Figure 20. Photoluminescence spectra of the films deposited onto glass substrates at different temperatures.

The crystal structure of $\beta\text{-In}_2\text{S}_3$ was characterized by a spinel structure with four empty tetrahedral sites. After excitation, these vacancies can play an important role in PL behavior, creating sulfur vacancies, indium interstitials (In_i) as donors, indium vacancies as acceptors (V_{In}) and oxygen in sulfur vacancies (OV_s). As shown in Figure 20, our films show interesting luminescence behavior compared to the bulk $\beta\text{-In}_2\text{S}_3$ that had non-luminescent behavior. Under 325 nm excitation, all films show a strong emission in the violet light band with twin peaks at 407 and 421 nm. This luminescence emission can be attributed to the In_2S_3 quantum-confined effects [31]. Another peak with lower intensity can be seen in the blue light region, located at 486 nm, accompanied with a shoulder one at 460 nm. These blue peaks may be due

to the recombination of electrons in sulfur vacancies with photo-excited holes [31]. Finally, a lower peak can be identified in the green emission band located at 530 nm resulting from the transition between indium vacancies and sulfur vacancies ($V_{In}-V_S$) [94].

Note also that indium oxide film present the same peaks to those of indium sulfide. In fact, the literature review show that In_2O_3 material can emit different luminescence band in the range of 400-600 nm, depending to the growth method and condition [95]. However, the slight shift observed may be attributed to the excitation source. Nevertheless, the higher violet and blue emissions compared to the green one suggests that our films could be a promising violet - blue light emitter.

On the other hand, it is well known that photoluminescence property of thin film materials has a close relation with the quality of the films, thus to their crystallinity. It can be noted that indium oxide film has the high PL peaks intensity, which indicate their higher quality. It is remarkable also, that films grown onto glass substrates at 200 and 400 °C have virtually the same intensity and the lower one. This observation reflects the lower quality of these films, which can be supported by the higher dislocation density of the film grown at 400 °C and to the amorphous nature of the film grown at 200 °C. In addition, it was shown that these two films present a similar behavior regarding n , k and ϵ_r as well as close E_o and E_u values, results that confirm the higher disorder, lower packing density and poor crystallinity, justifying the lower intensity of PL peaks of these two films.

Conclusion

In this study, β - In_2S_3 nanocrystalline thin films were successfully prepared using triphenylphosphine sulfide. From structural analysis, we can conclude that the best crystallinity and pure indium sulfide phase were obtained at 300 and 400°C with a tetragonal structure and preferred orientation along (109) plane. The morphological study confirms the formation of good coverage and high quality films that no depends on substrate nature and growth temperature. The band gap energy was found to be ≈ 2.7 eV for films deposited onto glass substrates, which makes them useful as buffer layers for photovoltaic applications. n , k , E_{osc} , E_{dis} , E_u parameters confirm the optoelectronic application of the resulting films. Photoluminescence spectroscopy shows that the obtained films have violet, blue, and green

emission. The obtained results shows that optical properties of β - In_2S_3 were highly affected by the substrate nature, while the effect of growth temperature cannot be always identified. The investigation of the density of states and band structure shows that band edge structure of β - In_2S_3 is the origin of their excellent optical properties, which mainly composed by S_{2-3p} states and In_{3-5s} states. Theoretical results are in good agreement with the experimental finding.

Acknowledgements

K. Assili and K. Alouani are very much thankful to Pr E Llobet for accepting the internship in his Research Group at the Department of Electronic, Electrical and Automatic Engineering of University Rovira i Virgili in Tarragona, Spain. Tunisian Ministry of Higher Education and Scientific Research (MHESR) is acknowledged for financial support through 'the Alternance Bourse' grant. This work has been funded in part by MINECO under grant no. TEC2015-71663-R and by AGAUR under grant no. 2017SGR418.

References

- [1] Y. G. Gololobov, L. F. Kasukhin, *Tetrahedron*, 48, 1992, 1353-1406.
- [2] *Ylides and imines of phosphorus*; Ed. A. William Johnson, Wiley, 1993, 614.
- [3] I. Haiduc, *Reference Module in Chemistry, Mol. Sci. Chem. Eng.*, 1, 2003, 349-376.
- [4] A. John, J. Glass, T. J. Spencer, *Thin Solid Films*, 315, 1998, 86–93.
- [5] K. Assili, K. Alouani, X. Vilanova, *Semicond. Sci. Technol.*, 32, 2017, 1–11.
- [6] K. Assili, O. Gonzalez, K. Alouani, X. Vilanova, *Arab. J. Chem.*, 2017.
- [7] N. OwusuBoadi, P. D. McNaughter, M. Helliwell, M. A. Malik, J. A.M. Awudza, P. O'Brien, *Inorg. Chim. Acta*, 453, 2016, 439-442.
- [8] G. Murtaza, M. Akhtara, M. A. Malika, P. O'Brien, N. Revaprasadu, *Mater. Sci. Semicond. Process.*, 40, 2015, 643–649.
- [9] S. Mahboob, S. N. Malik, N. Haider, C. Q. Nguyene, M. A. Malik, P. O'Brien, *J. Cryst. Growth*, 394, 2014, 39–48.
- [10] K. Seshan, *Handbook of thin film deposition processes and techniques*, Noyes publications William Andrew Publishing, 2001.
- [11] D. Barreca, C. Massignan, S. Daolio, M. Fabrizio, C. Piccirillo, L. Armelao, E. Tondello, *Chem. Mater.*, 13, 2001, 588-593.
- [12] T. S. Jeon, J. M. White, D. L. Kwong, *Appl. Phys. Lett.*, 78, 2001, 368-370.

- [13] M. L. Green, M. E. Gross, L. E. Papa, K. J. Schnoes, D. Brasen, J. Electrochem. Soc., 132, 1985, 2677-2685.
- [14] Y. Liu, E. Koep, M. Liu, Chem. Mater., 17, 2005, 3997-4000.
- [15] M. Zervos, P. Papageorgiou, A. Othonos, J. Cryst. Growth, 312, 2010, 656-661.
- [16] D. Byun, Y. Jin, B. Kim, J. K. Lee, D. Park, J. Hazard. Mater., 73, 2000, 199-206.
- [17] T. Ivanova, M. Surtchev, K. Gesheva, Mater. Lett., 53, 2002, 250-257.
- [18] M. Purica, E. Budianu, E. Rusu, M. Danila, R. Gavrilă, Thin Solid Films, 403 – 404, 2002, 485–488.
- [19] E. Aydin, M. Sankir, N. D. Sankir, J. Alloys Compd., 603, 2014, 119–124.
- [20] R. S. Becker, T. Zheng, J. Elton, M. Saeki, Sol. Energy Mater., 13, 1986, 97-107.
- [21] W. Rehwald G. Harbeke, J. Phys. Chem. Solids, 26, 1965, 1309-1318.
- [22] M. Amlouk, M. A. Ben Said, N. Kamoun, S. Belgacem, N. Brunet, D. Barjon, Jpn. J. Appl. Phys., 38, 1999, 26.
- [23] N. Barreau, A. Mokrani, F. Couzinié-Devy, J. Kessler, Thin Solid Films, 517, 2009, 2316–2319.
- [24] W. T. Kim, C. D. Kim, J. Appl. Phys., 60, 1986, 2631.
- [25] N. Barreau, Sol. Energy, 83, 2009, 363–371.
- [26] R. F. McCarthy, M. S. Weimer, J. D. Emery, A. S. Hock, A. B. F. Martinson, ACS Appl. Mater. Interfaces, 6, 2014, 12137–12145.
- [27] S. Chander, S. Choudhary, A. Purohit, N. Kumari, S. P. Nehra, M. S. Dhaka, Materials Focus, 4, 2015, 184–188.
- [28] M. Lajnef, H. Ezzaouia, The Open Applied Physics Journal, 2, 2009, 23-26.
- [29] N. Revathi, P. Prathap, Y. P. V. Subbaiah, K. T. R. Reddy, J. Phys. D: Appl. Phys. 41, 2008, 155404.
- [30] M. G. Sandoval-Paz, M. Sotelo-Lerma, J. J. Valenzuela-Jauregui, M. Flores-Acosta, R. Ramirez-Bon, Thin Solid Films, 472, 2005, 5–10.
- [31] G. Cao, Y. Zhao, Z. Wu, J. Alloys Compd., 472, 2009, 325–327.
- [32] S. Karthikeyan, A. E. Hill, R. D. Pilkington, Appl. Surf. Sci., 418, 2017, 199-206.
- [33] N. Bouguila, M. Kraini, I. Halidou, E. Lacaze, H. Bouchriha, H. Bouzouita, J. Elecron. Mater., 45, 2016, 829-838.
- [34] Y. Ji, Y. Ou, Z. Yu, Y. Yan, D. Wang, C. Yan, L. Liu, Y. Zhang, Y. Zhao, Surf. Coat. Technol., 276, 2015, 587-594.
- [35] A. M. A. Haleem, M. Ichimura, Thin Solid Films, 516, 2008, 7783–7789.
- [36] S. Lugo-Loredo, Y. Peña-Méndez, M. Calixto-Rodríguez, S. Messina-Fernández, A. Alvarez-Gallegos, A. Vázquez-Dimas, T. Hernández-García, Thin Solid Films, 550, 2014, 110–113.

- [37] P. Rao, S. Kumar, *Thin Solid Films*, 524, 2012, 93–99.
- [38] B. Yahmadi, N. Kamouna, R. Bennaceur, M. Mnari, M. Dachraoui, K. Abdelkrim, *Thin Solid Films*, 473, 2005, 201-207.
- [39] K. Assili, K. Alouani, X. Vilanova, *Semicond. Sci. Technol.*, 32, 2017, 115005.
- [40] G. A. Steigmann, H. H. Sutherland, J. Goodyear, *Acta Cryst.*, 19, 1965, 967-971.
- [41] S. J. Clark, M. D. Segall, C. J. Pickard, P. J. Hasnip, M. J. Probert, K. Refson, M. C. Payne, *Zeitschrift fuer Kristallographie*, 220, 2005, 567-570.
- [42] J. P. Perdew, K. Burke, M. Ernzerhof, *Phys. Rev. Lett.*, 77, 1996, 3865-3868.
- [43] Z. Wu, R. E. Cohen, *Phys. Rev. B.*, 73, 2006, 235116.
- [44] J. D. Head, M. C. Zerner, *Chem. Phys. Lett.*, 122, 1985, 264-270.
- [45] H. G. Tompkins, W. A. Mc Gahan, *Spectroscopic ellipsometry and reflectometry*, John Wiley & Sons Inc., New York, 1999.
- [46] M. Launay, F. Boucher, P. Moreau, *Phys. Rev B.*, 69, 2004, 035101.
- [47] M. Dressel, G. Gruner, *Electrodynamics of Solids: Optical Properties of Electrons in Matter*, Cambridge University Press, UK, 2002.
- [48] A. H. Reshak, S. A. Khan, *Comput. Mater. Sci.*, 78, 2013, 91.
- [49] A. Timoumi, H. Bouzouita, B. Rezig, *Aust. J. Basic Appl. Sci.*, 7(2), 2013, 448-456.
- [50] S. Rasool, G. P. Reddy, K. T. R. Reddy, M. Tivanov, V. F. Gremenok, *Materials Today: Proceedings*, 4, 2017, 12491–12495.
- [51] S. P. Nehra, S. Chander, A. Sharma, M. S. Dhaka, *Mater. Sci. Semicond. Process.*, 40, 2015, 26–34.
- [52] *Natl. Bur. Stand. (U.S.) Monogr.*, 25, 11, 1974, 30.
- [53] M. Afzaal, M. A. Malik, P. O'Brien, *Chem. Commun.*, 0, 2004, 334–335.
- [54] M. Ali Ehsan, M. M. Olmstead, T. A. N. Peiris, Z. Arifin, K. G. U. Wijayantha, M. Mazhar, V. McKee, *Dalton Trans.*, 42, 2013, 10919-10928.
- [55] R. Nomura, K. Konishi, H. Matsuda, *Thin Solid Films*, 198, 1991, 339-345.
- [56] M. Calixto-Rodriguez, A. Tiburcio-Silver, A. Ortiz, A. Sanchez-Juarez, *Thin Solid Films*, 480–481, 2005, 133–137.
- [57] M. Marezio, *Acta Cryst.*, 20, 1966, 723-728.
- [58] S. Fuyat., *Natl. Bur. Stand. (U.S.), Circ. 539.*, III, 12, 1954.
- [59] C. J. M. Rooymans *J. Inorg. Nucl. Chem.*, 11, 1959, 78-79.
- [60] N. S. Rampersadha, A. M. Ventera, D. G. Billing, *Physica B*, 350, 2004, e383–e385.
- [61] P. Scherrer, *Von Der Gesellschaft Der Wissenschaften Zu Gottingen, Mathematisch-Physikalische Klasse*, 1918, 98–100.

- [62] S. Thanikaikarasan, T. Mahalingam, K. Sundaram, A. Kathalingam, Y. D. Kim, T. Kim, *Vacuum*, 83, 2009, 1066–1072.
- [63] H. P. Klug, L. E. Alexander, Wiley, New York, 1974.
- [66] J. Henry, P. Prema, D. P. Padiyan, K. Mohanraj, G. Sivakumar, *New J. Chem.*, 40, 2016, 2609-2618.
- [67] C. Georges, R. Tena-Zaera, S. Bastide, J. C. Rouchaud, G. Larramon, C. Lévy-Clément, *J. Electrochem. Soc.*, 154, 2007, D669-D673.
- [68] P. A. Nwofe, K.T. Ramakrishna Reddy, J. K. Tan, I. Forbes, R.W. Miles, *Physics Procedia*, 25, 2012, 150 – 157.
- [69] Y. Ji, Y. Ou, Z. Yu, Y. Yan, D. Wang, C. Yan, L. Liu, Y. Zhang, Y. Zhao, *Surface and Coatings Technology*, 276, 25, 2015, 587-594.
- [70] D. Beena, K. J. Lethy, R. Vinodkumar, V. P. Mahadevan Pillai, V. Ganesan, D. M. Phase, S. K. Sudheer, *App. Surf. Sci.* 255 (2009) 8334–8342.
- [71] N. Revathi, P. Prathap, Y. P. V. Subbaiah, K. T. R. Reddy, *J. Phys. D: Appl. Phys.* 41, 2008, 155404.
- [72] Y. Nosaka, N. Ohta, H. Miyama, *J. Phys. Chem.*, 94, 1990, 3752.
- [73] C. D. Kim, H. Lirn, H. L. Park, H. Y. Park, J. E. Kim, H. G. Kirn, Y. G. Kim, W. T. Kim, *Thin Solid Films*, 224, 1993, 69-73.
- [74] T. Yoshida, K. Yamaguchi, H. Toyoda, K. Akao, T. Sugiura, H. Minoura, Y. Nosaka, *Proc. Electrochem. Soc.*, 37, 1997, 97-20.
- [75] C. Sanz, C. Guillén, M. T. Gutiérrez, *Thin Solid Films*, 511–512, 2006, 121-124.
- [76] S. K. Chong, S. N. A. Azizan, K. W. Chan, H. Nguyen, Z. Aspanut, C. F. Dee, S. A. Rahman, *Nanoscale Res. Lett.*, 8, 428, 2013, 1-9.
- [77] S. Naseem, I. A. Rauf, K. Hussain, N. A. Malik, *Thin Solid Films*, 156, 1988, 161-171.
- [78] N. Revathi, P. Prathap, K. T. R. Reddy, *Solid State Sci.*, 11, 2009, 1288–1296.
- [79] V. Senthilkumar, P. Vickraman, *Curr. Appl. Phys.*, 10, 2010, 880–885.
- [80] J. Ahmed, N. Seyhun, H. S. Ramaswamy, L. Giorgio, *Int. J. Food. Prop.*, 12, 2009, 896–909.
- [81] C. Talens, M. Castro-Giraldez, P. J. Fito, *LWT-Food Sci. Technol.*, 66, 2016, 622–628.
- [82] G. V. Barbosa-Canovas, P. Juliano, M. Peleg, Engineering properties of foods, in food engineering. In *Encyclopaedia of Life Support Systems (EOLSS)*; EOLSS: Oxford, UK, 2006.
- [83] Y. Zhang, J. Wu, L. Liang, G. Zhou, B. Jin, Y. Feng, *Sci. China Inform. Sci.*, 57, 2014, 1–8.
- [84] R. Fiore, Excerpt from complete *Circuit Designer’s Notebook*, Document #001-927, Rev. E, 1/05.

- [85] J. I. Pankove, *Opt. Processes Semicond.*, 1975, 91.
- [86] R. E. Mudgett, M. A., Rao, S. S. H., Rizvi, Eds.; Marcel Dekker: New York, NY, USA., 1986, 329–390.
- [87] G. Gavrilovs, S. Vitolina, The 51st Annual international scientific conference of Riga technical university section, Power and electrical engineering, 2010.
- [88] S. H. Wemple, M. DiDomenico, *J. Phys. Rev. B.*, 3, 1971, 1338-1351.
- [89] S. Gedi, V. R. M.Reddy, C. Park, J. Chan-Wook, R. K. T. Reddy, *Opt. Mater.*, 42, 2015, 468-475.
- [90] F. Urbach, *Phys Rev.*, 92, 1953, 1324.
- [91] S. J. Ikhmayies, R. N. Ahmad-Bitar, *J. Mater. Res. Technol.*, 2, 2013, 221.
- [92] A. Y. Abdellatif, H. M. Kotb, M. M. Haz, M. A. Dabban, *Mater. Sci. Semicond. Process.*, 30, 2015, 502.
- [93] L. A. Wahab, H. H. Amer, *Mater. Chem. Phys.*, 100, 2006, 430–433.
- [94] V. G. Rajeshmon, N. Poornima, C. S. Kartha, K. P. Vijayakumar, *J. Alloys Compnd.*, 553, 2013, 239–244.
- [95] D. Beena, K. J. Lethy, R. Vinodkumar, A. P. Detty, V. P. M. Pillai, V. Ganesan, *J. Alloys Compd.*, 489, 2010, 215–223.